Shelf Circulation and Cross-Shelf Transport out of a Bay Driven by Eddies from an Open-Ocean Current. Part I: Interaction between a Barotropic Vortex and a Steplike Topography

YU ZHANG

Massachusetts Institute of Technology, Cambridge, Massachusetts

JOSEPH PEDLOSKY

Woods Hole Oceanographic Institution, Woods Hole, Massachusetts

GLENN R. FLIERL

Massachusetts Institute of Technology, Cambridge, Massachusetts

(Manuscript received 29 April 2010, in final form 7 October 2010)

ABSTRACT

This paper examines interaction between a barotropic point vortex and a steplike topography with a bay-shaped shelf. The interaction is governed by two mechanisms: propagation of topographic Rossby waves and advection by the forcing vortex. Topographic waves are supported by the potential vorticity (PV) jump across the topography and propagate along the step only in one direction, having higher PV on the right. Near one side boundary of the bay, which is in the wave propagation direction and has a narrow shelf, waves are blocked by the boundary, inducing strong out-of-bay transport in the form of detached crests. The wave–boundary interaction as well as out-of-bay transport is strengthened as the minimum shelf width is decreased. The two control mechanisms are related differently in anticyclone- and cyclone-induced interactions. In anticyclone-induced interactions, the PV front deformations are moved in opposite directions by the point vortex and topographic waves; a topographic cyclone forms out of the balance between the two opposing mechanisms and is advected by the forcing vortex into the deep ocean. In cyclone-induced interactions, the PV front deformations are moved in the same direction by the two mechanisms; a topographic cyclone forms out of the wave–boundary interaction but is confined to the coast. Therefore, anticyclonic vortices are more capable of driving water off the topography. The anticyclone-induced transport is enhanced for smaller vortex–step distance or smaller topography when the vortex advection is relatively strong compared to the wave propagation mechanism.

1. Introduction

Circumpolar Deep Water (CDW) is ubiquitous over the west Antarctic Peninsula (WAP) shelf and within Marguerite Bay. The onshore intrusion of this warm and nutrient-rich water mass is important for the hydrographic structure on the shelf (Klinck 1998; Klinck et al. 2004) and supports a large population of Antarctic krill, an essential food source for many large Antarctic predators (Prezelin et al. 2000). Intrusions occur with high frequency (about four times a month) and in the form of small warm eddy-like structures (Moffat et al. 2009). Dinniman et al. (2011) found a strong correlation between the CDW intrusion and the wind stress along the shelf break and suggested that the short-duration wind events are responsible for the cross-shelf transport. However, their model resolution was not high enough to resolve baroclinic eddies in such a high-latitude region, so it remains a question whether the warm-eddy structure is a response to the wind forcing.

Another possible forcing of the CDW intrusion is the Antarctic Circumpolar Current (ACC), an eddying, energetic, wind-driven current flowing eastward around the Antarctic continent. The ACC is very close to the WAP shelf (Fig. 1): its southernmost front, the Southern ACC Front (SAACF), is right along the outer shelf break (Orsi

Corresponding author address: Yu Zhang, Department of Earth, Atmospheric and Planetary Sciences, Massachusetts Institute of Technology, 54-1421, Cambridge, MA 02139.
E-mail: sophiezy@mit.edu

DOI: 10.1175/2010JPO4496.1

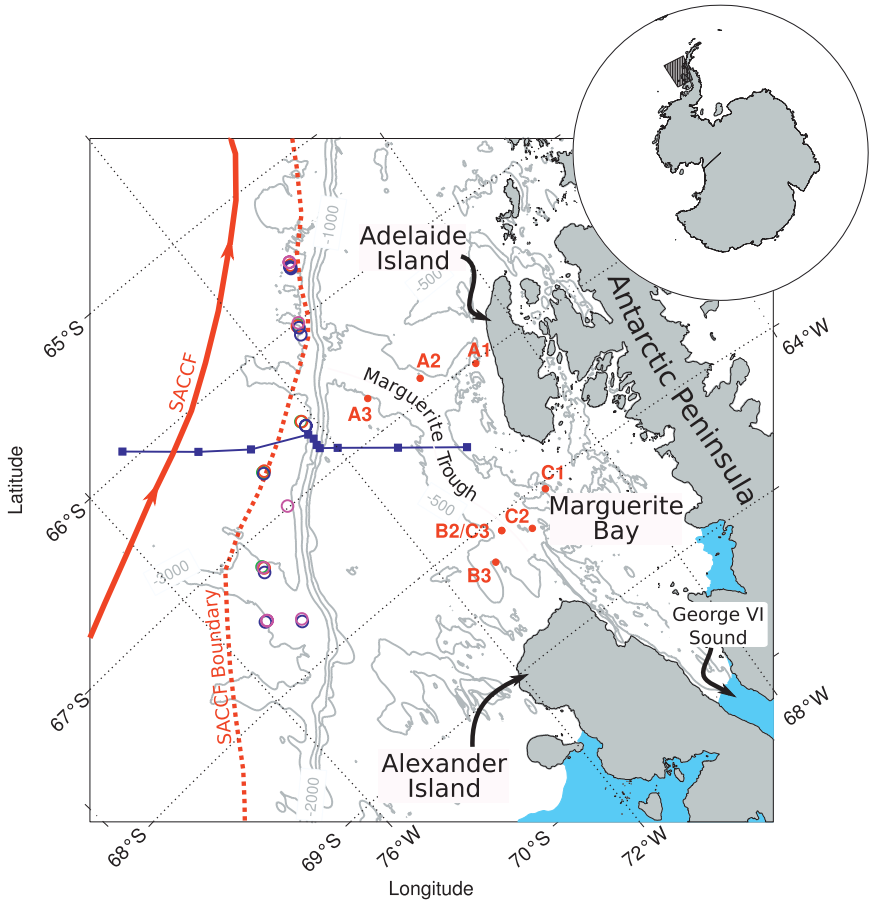

FIG. 1. The WAP shelf region is also the study region of the Southern Ocean Global Ecosystem Dynamics (SO GLOBEC). The red lines indicate the locations of the SACCF (solid line) and its southern boundary (dashed line) from historical data (Orsi et al. 1995). Also shown are the locations of the first 10 CTD casts conducted during the S04P cruise (blue squares), the SO GLOBEC moorings (red solid circles), and the CTD stations conducted off the shelf during the SO GLOBEC broad-scale cruises (open circles). This figure is from Moffat et al. (2009).

et al. 1995). In addition, the Antarctic Slope Front, a density front usually found around Antarctica, is absent off the coast of WAP, so eddies generated from the ACC can directly interact with the WAP shelf, driving the cross-shelf transport. Because both formation of the ACC eddies and their approach to the WAP shelf are intermittent, the ensuing eddy–shelf interaction and cross-shelf transport are naturally episodic. The time-dependent interaction between the ACC and the WAP shelf may also contribute to the mean circulation over the shelf, which consists of one or more gyres (Smith et al. 1999) and is speculated to provide the retention mechanism for Antarctic krill (Hofmann et al. 2002). Exploring the cross-shelf transport and the circulation over the shelf and in Marguerite Bay under the forcing of the ACC is the goal of the study. Our focus is on shelf geometry and shelf response to the intermittent offshore forcing. So far, neither aspect has been addressed in literature of eddy–topography interactions.

Earlier theoretical work often focused on only one aspect of the interaction process, which is either the eddy motion on the sloping bottom or the slope/shelf response to the offshore forcing. With a two-layer numerical model, Smith and O'Brien (1983) showed that, when an eddy moves over a slope, dispersion due to both planetary and topographic β effects gives rise to an asymmetric structure inducing different nonlinear propagation tendencies in anticyclones and cyclones. Cyclones are more likely to propagate onto the slope than anticyclones of equal strength. Louis and Smith (1982) studied topographic Rossby waves generated by a vorticity source on the slope in a homogeneous linear model. Chapman and Brink (1987) examined the slope/shelf response to the fluctuating offshore forcing in a linear model with continuous vertical stratification and arbitrary cross-shelf bottom topography. For forcing periodic in the alongshore direction and in time, the slope/shelf response varies with

the forcing frequency; for forcing by an anticyclonic eddy translating steadily in the alongshore direction, an alongshore jet is generated near the shelf break and is in the same direction as the propagation of topographic Rossby waves.

Wang (1992) studied the eddy–topography interaction that actively involves both the slope/shelf response and the eddy evolution. He examined the formation of topographic cyclones, the cross-topography transport, and the generation as well as the propagation of topographic Rossby waves in a one-layer ocean. More recently, White and McDonald (2004) studied interactions of point vortices in a two-layer fluid with a large-amplitude steplike topography. Although the topography is higher than the interface, the depth variation over the topography in the upper layer is small compared with the total layer thickness. The model results showed that cyclones propagate toward and even across the step, whereas anticyclones propagate away from the step because of the dipole formation. Frolov et al. (2004) examined the interaction of a Loop Current eddy (LCE)–type anticyclone with a realistic western-boundary topography that is high enough to intersect layer interface in a two-layer ocean model. They showed that the anticyclonic eddy generates a surface cyclone from the slope and then moves together with it. In the situation of a narrow shelf, advection of surface eddies by equivalent of image vortices becomes significant.

In the aforementioned studies, the shallow area is either infinite (Wang 1992) or bounded by a straight coast parallel with topography (Frolov et al. 2004), the effect of which is straightforward: to make the eddy translate along the coast. Eddies interacting with topography are usually prescribed as initial or boundary conditions. The intermittency of the process due to the intermittent occurrence of the forcing eddy was not considered, although it is typical for cross-slope transport in many coastal regions (Garfield and Evans 1987). For such reason, we decide to explore the fundamental idea by studying models with very idealized configurations. Zhang (2009) and Zhang et al. (2011, manuscript submitted to *J. Phys. Oceanogr.*, hereafter ZPF) consider a model ACC driven by a steady wind forcing, flowing eastward in a zonally periodic channel. Near the southern boundary, the middle part of which is indented shoreward, lies a zonally uniform slope representing the topography of the WAP shelf. The flat-bottomed region between the shelf break and the curved southern boundary represents Marguerite Bay. Topographic features over the WAP shelf, such as Marguerite Trough, are ignored for simplicity. However, the interactions between the offshore eddy field and the fluid in the shallow bay can best be understood by examining the effects of single eddies.

In this paper, we investigate only the effect of the shelf geometry without considering the intermittency of the forcing. The cross-shelf transport is driven through the interaction between a barotropic point vortex and a steplike topography on a quasigeostrophic f plane. To the south of the topography, the shallow area is bounded by an indented coast into a bay. One may question the relevance of the model because it is highly simplified from the oceanographic context. However, the setting of the model enables us to study the eddy–topography interaction and its relation to the shelf geometry in the simplest way. As in Wang (1992), waves are found to propagate along the step in only one direction, having higher potential vorticity (PV) on the right. We find the single propagation direction of topographic waves is responsible for the fundamental difference between the anticyclone- and cyclone-induced interactions. With the presence of a bay, the propagation of the waves tends to be prohibited by the curved coast, resulting in wave–boundary interaction and strong out-of-bay transport. The resultant strong exchange between the deep and the shallow region only occurs near one side of the bay. In the current paper, we assume the model domain is in the Northern Hemisphere with positive f_0, so topographic waves propagate eastward along the step with shallow region to its south and interact with the eastern side of the bay's boundary. In the Southern Hemisphere, however, it is the western side of Marguerite Bay that may have strong wave–boundary interaction and cross-isobath transport because f_0/H is smaller over the shelf than in the deep ocean and topographic waves propagate westward along the isobath.

In the companion paper (ZPF), factors ignored in this paper—baroclinicity, smooth topography, wind-driven current, etc.—are considered, which make the model much more readily associated with the real ocean. The fundamental mechanism presented in this paper, the wave–boundary interaction inducing strong asymmetry inside the bay is found crucial for the ACC-driven shelf circulation and cross-shelf transport in the more realistic model.

The paper is organized as follows: In section 2, we examine the influence of a curved coastline on the free, linear topographic Rossby waves using the WKB approximation approach. In section 3, we present experiments of vortex–step interactions with a nonlinear contour dynamics model (Stern and Flierl 1987; Wang 1992). The reason for qualitative difference between anticyclone- and cyclone-induced interactions is explored, and the effects of various parameters like the height of the topography and the initial location of the vortex are investigated. Conclusions and discussions are provided in section 4.

2. Free, linear topographic Rossby waves

Within the linear framework, we find an analytical solution for waves supported by a step topography and modified by a curved coast. Let us consider a one-layer

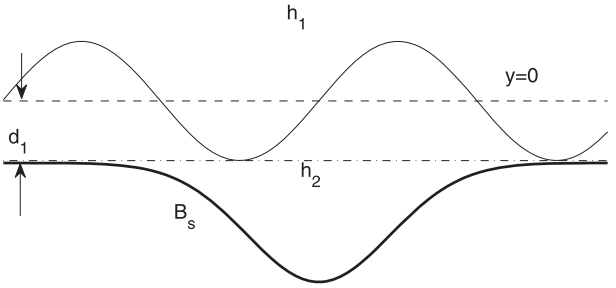

FIG. 2. A schematic of the model domain bounded by a curved southern boundary B_s (thick solid line). The dashed line denotes the steplike topography along $y = 0$; the dashed–dotted line denotes the latitude of the bay opening with distance d_1 to the step; the thin solid line denotes the PV front deformed from $y = 0$. Water depth is h_2 to the south of the topography and h_1 to the north of the step.

ocean on the *f* plane in the Northern Hemisphere, where a steplike topography is located at $y = 0$, separating the region into two parts: a deep area with constant depth h_1 in the north and a shallow area with depth h_2 in the south (Fig. 2). The shallow region is bounded by a curved coast at $y = B_s(x)$, which is bent southward and forms a bay-shaped shelf. In the north, however, the domain is assumed boundless to single out the impact of the curved coast on the topography-supported waves. A PV front is induced by the abrupt depth change across the topography and lies along the step with higher PV in the shallow region when the ocean is at rest. Once motions are excited near the step, the PV front is deformed and water columns crossing the topography generate relative vorticity to conserve PV in the absence of any frictional forcing. The relative vorticity equals to $f_0[(h_1/h_2) - 1] > 0$ if the water column crosses the step from the south and $f_0[(h_2/h_1) - 1] < 0$ if it gets into the shallow region from the north. The PV front is further advected by the velocity field associated with the relative vorticity, and the front's meridional location l varies both in x and time. If we assume the step is small compared with the ocean depth and the meridional scale of the PV front deformation is small compared with its zonal scale, the relative vorticity generated by a water column that has crossed the step has a simple relation with l (appendix A):

$$\nabla^2\psi = \Delta q l \delta(y), \tag{1}$$

where $\Delta q = (f_0/H_0)(h_1 - h_2)$ measures the amplitude of the PV jump across the step and H_0 is the approximate ocean depth, $h_1 \approx h_2 = H_0$. Once the streamfunction is known, the evolution of the PV front is obtained through the following equation:

$$\frac{\partial l}{\partial t} + u_l \frac{\partial l}{\partial x} = v_l, \tag{2}$$

where $u_l = -[\partial\psi(x, l)/\partial y]$ and $v_l = -[\partial\psi(x, l)/\partial x]$. Under the previous assumption that the PV deformation is small compared with its zonal length, the equation is linearized as

$$\frac{\partial l}{\partial t} = v_0, \tag{3}$$

where v_0 is the velocity at $y = 0$ instead of $y = l$. The solution of ψ also has to satisfy the boundary condition at $y = B_s < 0$ and $y \to \infty$,

$$\begin{aligned} &\psi(x, B_s) = 0, \\ &\psi(x, \infty) \text{ is finite.} \end{aligned} \tag{4}$$

Assuming the zonal length scale of the wave is small compared with that of the variation of B_s, we apply the WKB approximation and find solutions in form of $l = l_0(x) \exp[i\theta(x) - i\omega t] + \text{c.c.}$ and $\psi = A \exp[i\theta(x) - i\omega t]\phi(y) + \text{c.c.}$, where c.c. denotes the complex conjugate and l_0, A, and $k = (d\theta/dx)$ are slow functions of x. Readers are referred to appendix A for a detailed description of the solution method, and here we focus on the property of the waves supported by the step and constrained by the curved southern boundary.

First of all, wave motions are trapped at the step: amplitudes of the streamfunction decay away from the step as e^{-ky} in the deep area and $\sinh k(y - B_s)$ in the shallow region. The wave frequency $\omega = (\Delta q/2)[1 - e^{2kB_s(x)}]$ and the wavenumber k have the same sign in the Northern Hemisphere ($\Delta q > 0$) but opposite signs in the Southern Hemisphere ($\Delta q < 0$). Therefore, the topographically trapped waves always propagate along the topography with higher PV on the right, regardless of the sign of f_0 as well as the orientation of the topography. If the topography extends meridionally with shallow area on its west, as the continental slope off the northeast coast of North America does, topographic waves propagate equatorward. These waves are similar to the planetary Rossby waves in the sense that both propagate along PV contours with higher PV on the right, so topographic waves are also called topographic Rossby waves. The energy is transported along the step and with the speed $c_g = -\Delta q B_s e^{2kB_s}$; the propagation direction is the same as that of the phase.

The dispersion relation of the wave depends explicitly only on x, so the wave frequency remains constant as the wave propagates while the wavenumber varies as $1/|B_s|$, which means the wave becomes shorter as the shelf width decreases. The wave amplitude, A, is proportional to Δq, implying that waves are bigger and more nonlinear as the depth difference across the step is increased. Here, A is also found to vary like $\sqrt{|B_s|}$, but the steepness, the ratio

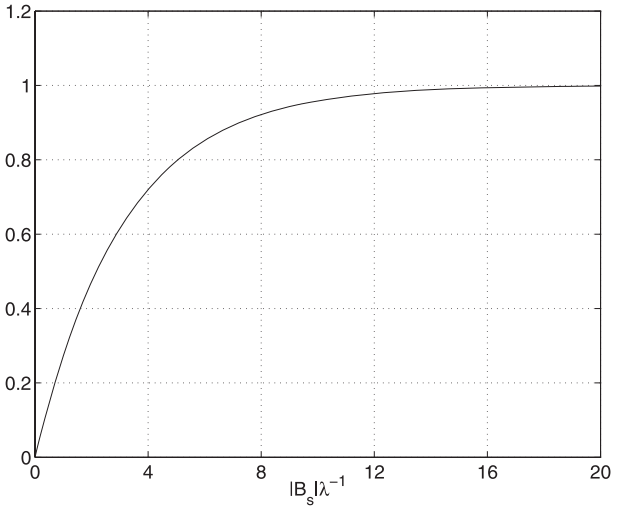

FIG. 3. The frequency of the free, linear topographic Rossby waves scaled by $\Delta q/2$ plotted against the ratio between the shelf width $|B_s|$ and the wavelength $\lambda = 2\pi/k$.

between the amplitude and the wavelength kA, changes as $1/\sqrt{|B_s|}$, suggesting that the waves become steeper and more inclined to break toward the narrow-shelf region despite the decrease of the wave amplitude. These effects of varying the shelf width diminish when the wave is much shorter than the shelf width $|B_s|$. As shown in Fig. 3, when the ratio between $|B_s|$ and the wavelength is greater than 16, the wave properties become independent of shelf width variations and the frequency is reduced to $\Delta q/2$, which is the same as that of the escarpment waves in an infinite domain (Wang 1992).

3. Nonlinear interaction between a barotropic point vortex and a small steplike topography

In this section, the nonlinear interaction between a barotropic vortex and a step is studied numerically in a zonally periodic channel ($x \in [0, a]$) with two boundaries at $y = B_n$ and $y = B_s$. The vortex–step interaction is dynamically similar to the interaction between a vortex and a PV front induced by a discontinuity in shear (Bell 1990; Stern and Flierl 1987; Stern 1991; Bell and Pratt 1992), and the contour dynamics approach is adopted (Stern and Flierl 1987; Wang 1992). The quasigeostrophic approximation is applied to the study, under which the height of the step is assumed small compared with the depth of the model ocean. This approximation is not expected to cause qualitative changes of results as suggested by Wang (1992) but greatly simplifies the solution method (appendix C). The vorticity equation of the problem is the following:

$$\nabla^2\psi^* = \Gamma^*\delta(x^* - X^*, y^* - Y^*) + q^*(x^*, y^*), \quad (5)$$

where Γ^* is the circulation of the point vortex located at (X^*, Y^*) and q^* is the relative vorticity generated by all water columns that have crossed the step from either side. We introduce the following scaling in (5):

$$x^*(y^*) = Lx(y), \; t^* = Tt. \quad (6)$$

The length scale L is defined as $\sqrt{S}$, where S is the area of the bay and the time scale T is defined as L^2/Γ^*. We further scale q^* and ψ^* as $q^* = (\Gamma^*/L^2)q(x, y)$ and $\psi^* = \Gamma^*\psi(x, y)$. Notice that the dimension of the Dirac delta function $\delta(x^*, y^*)$ is $1/L^2$ and the nondimensional form of (5) is

$$\nabla^2\psi = \delta(x - X, y - Y) + q(x, y). \quad (7)$$

As described in appendix C, the streamfunction corresponding to the PV front deformations is equal to an integral over the forcing area, $\psi_p = \iint_A q(\xi, \eta)G(x, y, \xi, \eta)\, d\xi\, d\eta$, where G is the Green's function of a source at (ξ, n). With the assumption that the depth difference across the step is small compared with the total depth, relative vorticity generated by a water column crossing the step has constant magnitude but opposite signs depending on at which side of the topography the water column is originally located. The previous integral is reduced to $\psi_p = \Delta q \iint_{A^+} G(x, y, \xi, \eta)\, d\xi\, d\eta - \Delta q \iint_{A^-} G(x, y, \xi, \eta)\, d\xi\, d\eta$, where A^+ denotes the total area of water columns from the shallow region and A^- denotes the total area of water columns from the north. The nondimensional parameter Δq is relevant to the problem because it determines the strength of the topography and probably the magnitude of the response as well. Its dimensional form is $\Delta q^* = (f_0/H_0)(h_1 - h_2)$ and is scaled as $\Delta q^* = (\Gamma^*/L^2)\Delta q$.

The evolution of the PV front is described by the following equation:

$$\frac{\partial l}{\partial t} + u_l\frac{\partial l}{\partial x} = v_l, \quad (8)$$

where $u_l = -\partial\psi(x, l)/\partial y$ and $v_l = -\partial\psi(x, l)/\partial x$ are velocities at the PV front. The vortex itself is also advected by the velocity field,

$$\frac{dX}{dt} = u(X, Y) = -\frac{\partial\psi(X, Y)}{\partial y},$$
$$\frac{dY}{dt} = v(X, Y) = -\frac{\partial\psi(X, Y)}{\partial x}. \quad (9)$$

Assuming no mean flow in the channel, we have the streamfunction equal to 0 at both boundaries; that is,

$$\psi = 0 \quad \text{at} \quad y = B_n \quad \text{and} \quad y = B_s. \tag{10}$$

The northern boundary is zonal, whereas the meridional location of the southern boundary B_s varies as a Gaussian function,

$$B_s = -d_1 - d_2 \exp[-w(x - 0.5a)^2] < 0, \tag{11}$$

indicating a bay area formed between the step and the shoreward-bent coastline. The bay's meridional depth d_2 is fixed at 0.5; the bay's zonal length scale is determined by w, which is set as 1. Compared with Marguerite Bay, which is about 200 km long and 100 km wide, the bay in the model is much shallower. Meanwhile, under the barotropic assumption, the decay length scale of the forcing eddy is on the order of the external deformation radius and much greater than that of mesoscale eddies. Both of these two features may cause unrealistically strong forcing as well as response near the base of the bay, so a quantitative comparison with real ocean has to be made carefully. The latitude of the bay opening (the dashed–dotted line in Fig. 2) is parallel with the step (the dashed line in Fig. 2), and the distance between the two is d_1. It is set either as 0.01 or around 0.2 in our calculations; the second value is more realistic for Marguerite Bay because the distance between the shelf break and the opening of Marguerite Bay is around 100 km, similar to the bay's depth. The length of the channel a is set as 16π, and the reason for that is explained in appendix B. Effects of the northern boundary on the vortex–step interaction and the vortex's motion are not focus of the present study, so we move the northern boundary very far in the north by specifying $B_n = 100$, much greater than $|B_s|$.

Equations (7)–(10) are solved numerically using the method described in appendix C. In extended integrations, contour surgery (Dritschel 1988) is employed whenever necessary. For example, if two successive elements of the PV contour are almost coincident with each other, looking like a tail, the snipping adjustment is applied to the front, cutting off the tail and connecting the two parts where the tail starts.

In the following sections, we explore the numerical results and analyze their dependence on various parameters such as the strength of the step topography, the initial location of the vortex, etc. It should be noted that throughout the paper the Coriolis parameter f_0 is positive and the channel with the bay is in the Northern Hemisphere, where anticyclones have clockwise circulation and cyclones the anticlockwise circulation. The PV is higher in the shallow area and decreases northward across the step. Water columns crossing the step from the south are stretched and generate positive relative vorticity with counterclockwise circulation, whereas water columns entering the shallow region from the north are squeezed and generate negative relative vorticity. The interaction within the same domain in the Southern Hemisphere is exactly the same if we interchange the east and west directions.

a. Asymmetry between the western and the eastern boundary of the bay

As demonstrated in section 2, linear waves propagate along the step to the east in the current configuration, having amplitudes decay away from the topography. In the presence of a curved coast along which the width of the shelf varies, the waves are shortened and more inclined to break approaching the narrow-shelf region. Properties of the nonlinear topographic waves, revealed by solutions of the full nonlinear equation in the absence of the forcing vortex, are our focus of this section. In Figs. 4 and 5, we examine two results of different distances between the northern edge of the bay, which is also the straight coast, and the step. In both figures, the PV front is initially perturbed as a shoreward trough in the west and a seaward crest in the east. After $t = 0.0$, the initial wave propagates eastward followed by generation of new waves as water particles move back and forth across the step. The shoreward motion of the water particles is more likely to be prohibited by the boundary in the narrow-shelf region (Fig. 4). The initial trough is blocked and squeezed against the eastern boundary by the following crest, inducing the shortening of the wavelength as the linear analysis predicted. The decrease of the wavelength enhances the meridional velocity and tends to amplify the deformations of the PV front (Fig. 6). Wave crests thrust farther into the deep ocean as they propagate eastward and pass the eastern edge of the bay, after which they move along the coast as isolated cyclones under the effect of the wall. At some point, as shown by Fig. 4d, the crests grow so large that they close upon themselves and break off from the PV front. Troughs squeezed against the boundary extend themselves southward into the bay, carrying the deep-ocean water onto the shelf. The blocking of the trough by the wall and the escape of the crest from the bay occur from time to time as waves are generated continuously and propagate toward the east. If the PV difference across the step is increased by increasing the topography, the eastward propagation of waves is faster, so the PV front near the eastern edge of the bay quickly develops complex patterns and the crest detachment occurs more frequently. Because of the single propagation direction of the topographic Rossby waves, the wave–boundary interaction only takes place in the propagation direction of waves, causing big deformations of the PV front as well as persistent yet episodic out-of-bay transports near the eastern

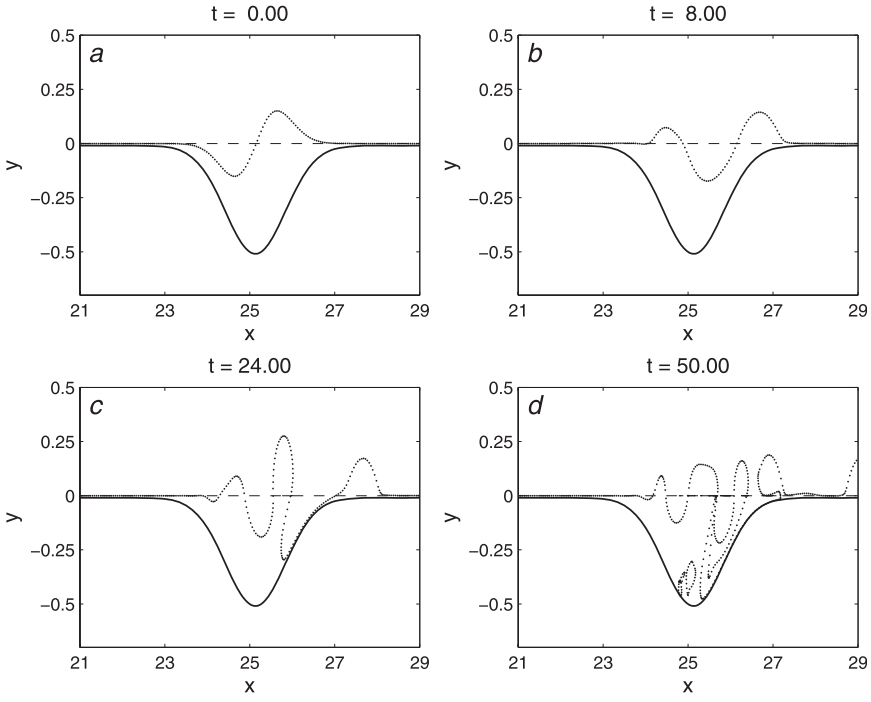

FIG. 4. Time evolution of the PV front (lines made up of dots) in the case with no point vortex and vanishingly small minimum shelf width $d_1 = 0.01$: t = (a) 0.00, (b) 8.00, (c) 24.00, and (d) 50.00 The dashed line denotes the position of the step topography, which is coincident with the coast outside the bay.

edge of the bay. The other side of the bay is much more quiescent with small PV deformations.

The strength of the wave–boundary interaction depends on the minimum shelf width d_1, because the interaction is induced by the prevention of wave propagations by the coast. Increasing d_1 weakens the coast's effect as in Fig. 5, where the PV front deformations propagate more regularly eastward with little nonlinearity. In this sense, increasing the minimum shelf width strengthens the propagation mechanism of the linear topographic Rossby waves and weakens the wave–boundary interactions. As noted before, $d_1 = 0.2$ is closer to the condition of Marguerite Bay, but that does not mean the wave–boundary interaction in Marguerite Bay must be insignificant as in Fig. 5. Remember the interaction in this paper is induced by a single eddy, whereas the WAP shelf is probably continuously influenced by the ACC, which excites the topographic waves continuously and probably at multiple sites over the shelf. Under the cumulative effect of the wave–boundary interaction, the PV front deformations may still grow into large amplitudes, producing strong out-of-bay transport. In ZPF, the out-of-bay transport caused by the wave–boundary interaction under the ACC's continuous forcing is actually very strong and comparable to that directly forced by the ACC eddies.

b. *Differences between anticyclone- and cyclone-induced interactions*

There are two mechanisms controlling the evolution of the PV front: the propagation of topographic Rossby waves and advection by the point vortex. The former has been examined in section 3a; the latter can be understood in two cases with no topography, very small minimum shelf width ($d_1 = 0.01$), and forcing vortices of opposite signs. Figure 7 shows the time evolution of the interface originally along $y = 0$ in the two cases that have the vortex initially located at ($X_0 = 8\pi$, $Y_0 = 1.0$) and face the southern tip of the bay. The initial zonal advection within the bay induced by the vortex is symmetric about the bay's meridional axis along $X_0 = 8\pi$. In the absence of the topography, the interface deforms without inducing relative vorticity, so it is passively advected by the vortex which meanwhile moves under the wall's influence.

The effect of the wall on the vortex motion as well as the circulation can be understood as follows: Let us consider a point vortex in a semi-infinite domain bounded by a straight wall. The resultant circulation is equivalent to the sum of circulations of two vortices: one is the original vortex and the other is an image vortex, which has the opposite strength and is located at the symmetric

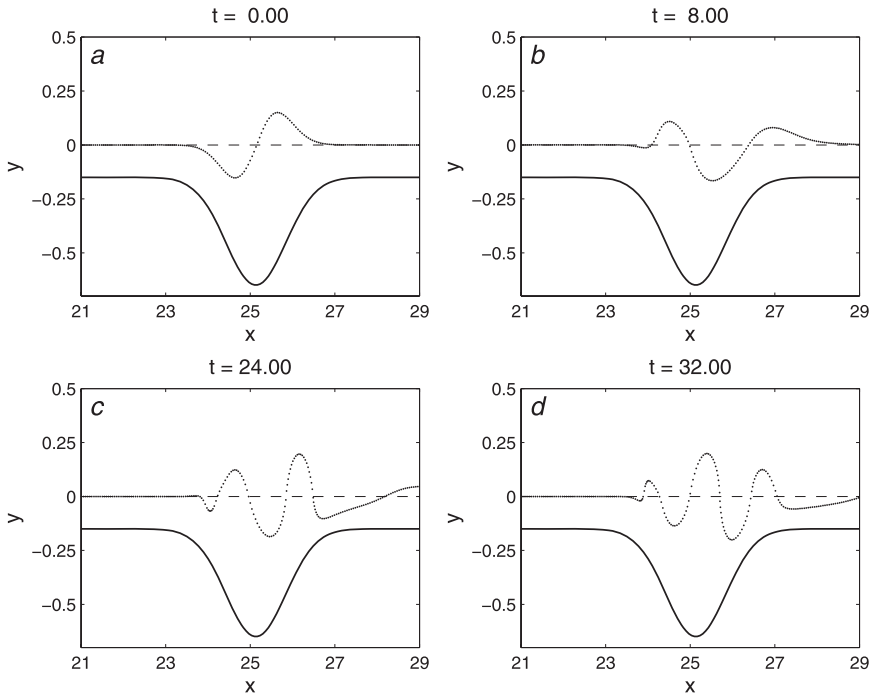

FIG. 5. Time evolution of the PV front (lines made up of dots) in the case with no point vortex and finite minimum shelf width $d_1 = 0.15$: t = (a) 0.00, (b) 8.00, (c) 24.00, and (d) 32.00. The dashed line denotes the position of the step topography.

position of the original vortex about the wall. The normal circulation component of the image vortex cancels that of the original vortex at the wall, so the no-normal flow boundary condition is satisfied. The along-wall circulation, however, is doubled from that of the original vortex. Moreover, the original vortex itself is advected by the image vortex in the same direction as the along-wall circulation. For example, if the original vortex is anticyclonic and advects the fluid near the wall westward (the wall is to the south of the vortex in the Northern Hemisphere), then the image vortex is cyclonic and advects the original vortex westward as well. Similarly, in Fig. 7, the anticyclonic vortex is advected westward while the cyclonic vortex is advected eastward by image vortices.

In the anticyclone-induced case (Fig. 7a), the vortex initially develops a crest in the west and a trough in the east. As time goes on, the trough is deepened while the crest is stretched northward and meanwhile advected westward. When the trough attaches to the boundary everywhere within the bay, all the bay water is squeezed into the crest, which is deformed into a long and thin filament encircling the anticyclone clockwise. The evolution of the interface in the cyclone case (Fig. 7b) is completely antisymmetric to the anticyclone case: the crest evolves into a filament containing all the bay water and stretched counterclockwise around the cyclone. With vortices located fairly close to the coast, the effect of the boundary is prominent in advecting them along the wall with two symmetric trajectories about the initial location ($X_0 = 8\pi$, $Y_0 = 1.0$) (Fig. 8a).

In interactions that have both topography and vortices, the two mechanisms coexist, and the antisymmetry described above is broken because of the single propagation direction of the topographic waves. Figure 9 shows the results of two "standard" cases with ($X_0 = 8\pi$, $Y_0 = 1.0$),

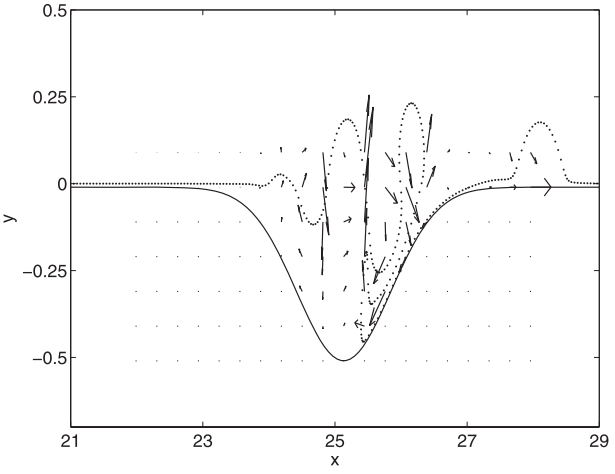

FIG. 6. The velocity field superimposed on the PV front deformations at $t = 32.0$ in the same case as in Fig. 4.

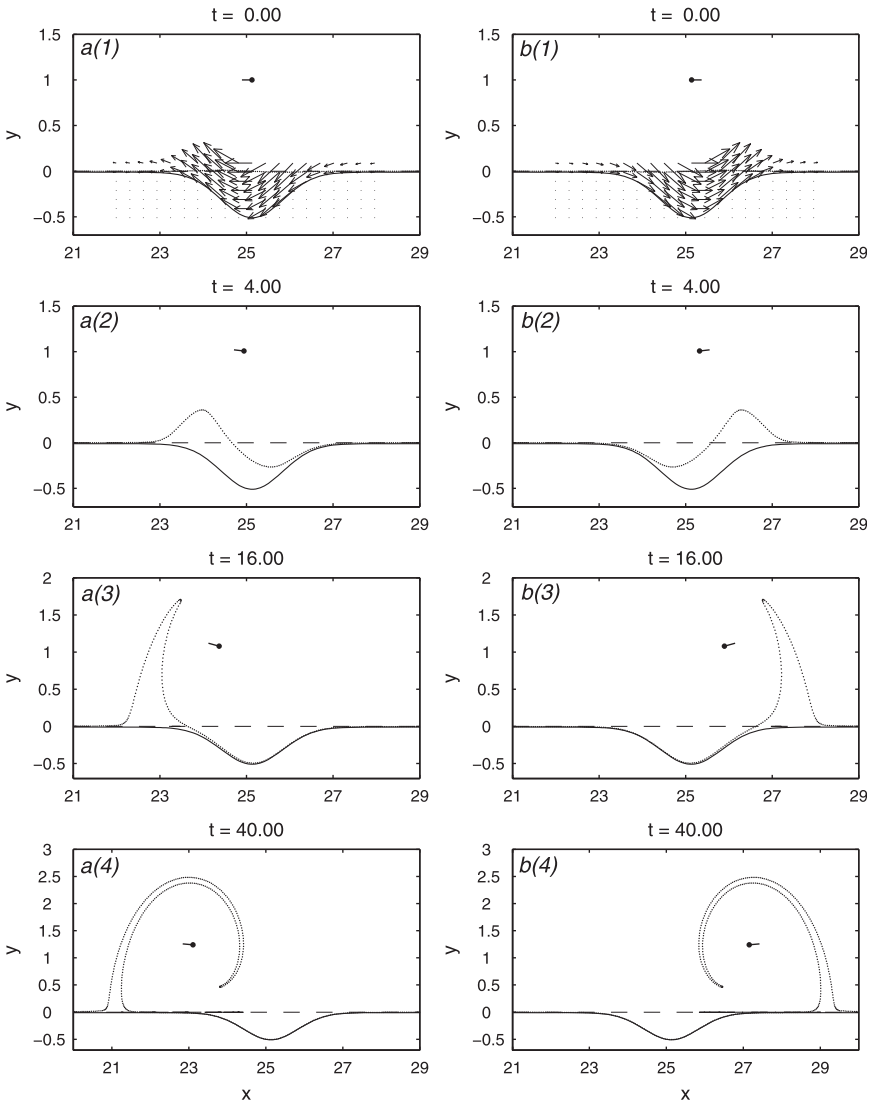

FIG. 7. Time evolution of the PV front (lines made up of dots) in the limit of 0 topography in (left) the anticyclone-induced case and (right) the cyclone-induced case: (top to bottom) t = 0.00, 4.00, 16.00, and 40.00. The velocity field within the bay at the beginning is shown with arrows. The velocity vector of the vortex is illustrated by a bar starting from a dot representing the location of the vortex.:

and $|\Delta q| = 1$. The two cases only differ in the sign of the vortex. In the anticyclone case (Fig. 9a), the vortex advects the PV structure westward, opposite to the propagation direction of the topographic Rossby waves, and the two mechanisms compete with each other with comparable strengths. As a consequence of the balance between the two, the western foot of the initial crest becomes stagnant and is not advected far from its original location. To the east of it, the initial trough is quickly advected southwestward along the bay's boundary, approaching the western foot and squeezing more and more bay water into the crest. The crest therefore develops into a big head and then separates from the front under the advection by the vortex. After separation, this topographic cyclone and the original anticyclonic vortex form a dipole, moving into the deep ocean. The shallow-ocean water within the bay has been completely replaced with the deep-ocean water, so the circulation within the bay is equivalent to that of a large anticyclonic eddy, directed eastward near the opening and westward in the interior.

In the cyclone case (Fig. 9b), the PV front is advected eastward by both mechanisms. The eastward advection of the initial trough is so strong that it touches the bay's eastern boundary before it gets to the bottom of the bay,

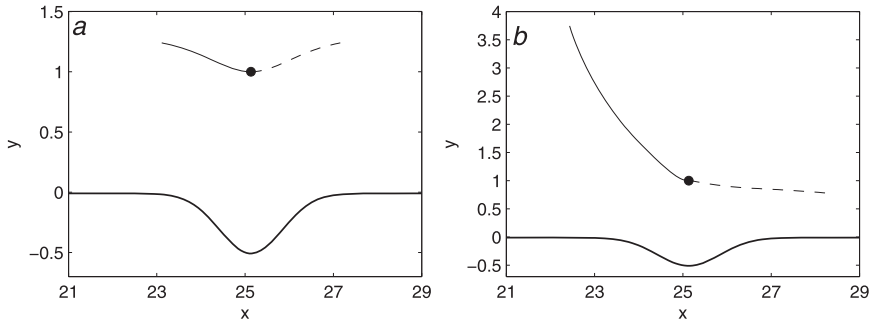

FIG. 8. Vortex trajectories in (a) the case with no topography and (b) the case with $\Delta q = 1$. Trajectories of the anticyclonic vortex are denoted by solid lines; trajectories of the cyclonic vortex are denoted by dashed lines. Thick solid lines illustrate the coast.

leaving a large amount of water trapped within the bay between the front and the coast. Because the shelf width outside the bay is nearly zero in these two cases, the wave breaks at the bay's eastern edge and the detached crest moves past the eastern edge translating eastward along the coast. The circulation within the bay is also clockwise because of the existence of the deep-ocean water, but the amplitude is smaller than that in the anticyclone case.

In addition to the PV front evolutions, the motions of vortices are also different in the anticyclone and cyclone case and are no longer antisymmetric (Fig. 8b). In the anticyclone case, the vortex first moves northwestward as advected by the anticlockwise circulation of the seaward PV deformation near the topography. After the topographic cyclone forms and separates from the front, the vortex moves along a clockwise path as it pairs with the cyclone. In the cyclone-induced case, the vortex moves eastward because of both the shoreward deformation of the PV front and the image vortices; meanwhile, it also slowly approaches the coast under the influence of the seaward deformation of the PV front that leads the vortex in the east.

Although a topographic cyclone forms and exits the bay in both anticyclone- and cyclone-induced interactions, the generation mechanisms are different. In the anticyclone-induced interactions, the topographic cyclone results from the balance between the wave propagation and the vortex advection, whereas, in the cyclone-induced interactions, the topographic cyclone forms from wave breaking over the narrow shelf. Furthermore, in the anticyclone-induced interactions, the topographic cyclone is not only much bigger but also translated farther into the deep ocean, whereas, in the cyclone-induced interactions, the topographic cyclone is restricted to the coast. Therefore, the cross-topography transport is more efficient in anticyclone-induced interactions, which are the subject of the following discussion.

The minimum shelf width d_1 has important influence on the competition between the two governing mechanisms because, as described in section 3a, increasing d_1 tends to strengthen the propagation of topographic Rossby waves and weaken the wave–boundary interactions. Shown in Fig. 10 are two anticyclone-induced interactions with different minimum shelf width. The initial along-step advections by the vortices are the same in the two cases because the vortices are located at the same position. However, because of the larger distance between the vortex and the bay in the case with $d_1 = 0.2$, the initial trough extends more slowly toward the bay's boundary. More of the shallow seawater is taken off the topography from outside the bay rather than inside the bay. Although the total cross-topography transport is bigger in the wide-shelf case, the out-of-bay transport is much less; in other words, the bay water is not completely replaced with the deep-ocean water as in the small d_1 case. Furthermore, in the bigger d_1 case, the volume of the topographic cyclone that is swept away by the forcing vortex is smaller and its formation process is longer. A large amount of the shallow seawater that has been taken off the step is left behind, moving around the bay because of the interaction with the anticyclonic vorticity of the deep-ocean water within the bay (after $t = 30.0$, but it is not shown in Fig. 10b). The shelf circulation at $t = 30.0$ is the result of the interaction between a cyclonic eddy to the north of the step and an anticyclonic eddy inside the bay. The strongest current therefore occurs near the bay opening, flowing to the northeast.

c. *Dependence of the anticyclone-induced interactions on the topography strength Δq and the initial meridional location Y_0*

The area of the bay and the circulation of the vortex have been used to nondimensionalize the governing equation of the problem. The remaining independent parameters are the vortex initial location (X_0, Y_0) and the PV jump Δq.

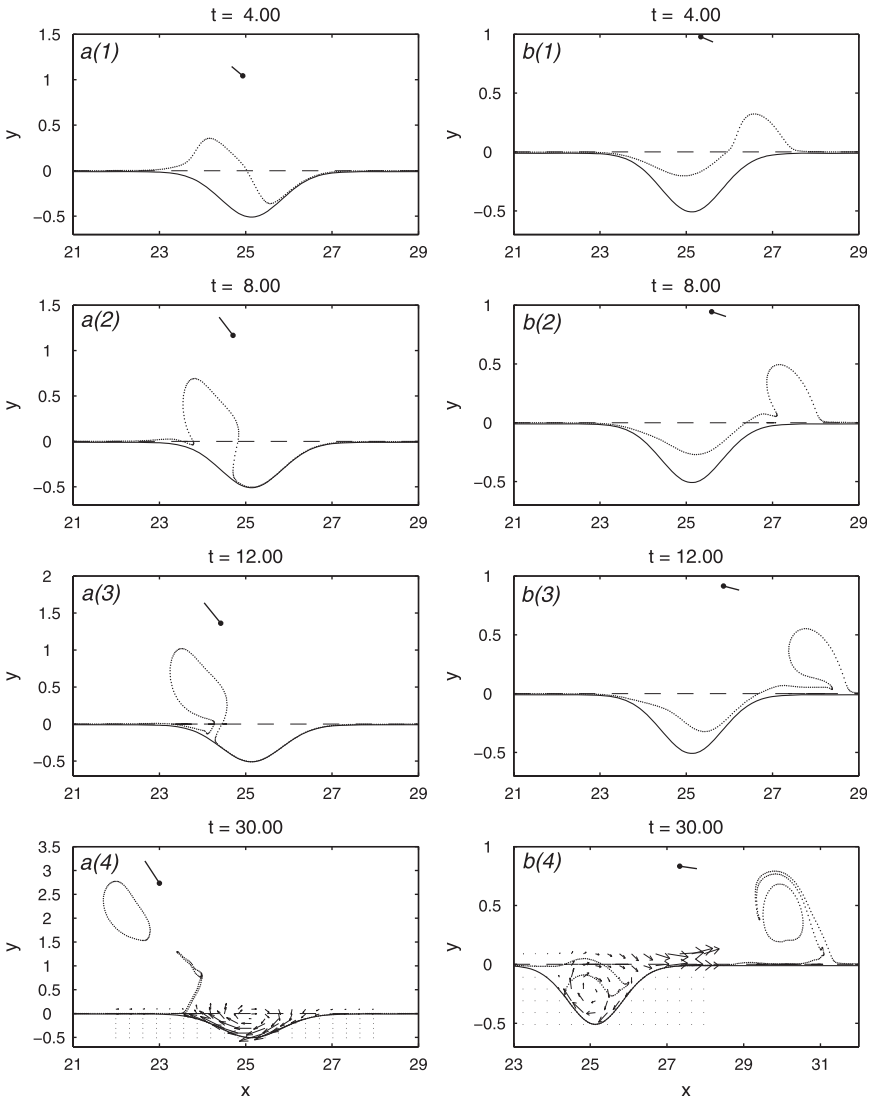

FIG. 9. Time evolution of the PV front (lines made up of dots) in standard cases with $\Delta q = 1$ and ($X_0 = 8\pi$, $Y_0 = 1.0$) in (left) the anticyclone-induced interaction and (right) the cyclone-induced interaction:(top to bottom) $t = 0.00$, 8.00, 12.00, and 30.00. The velocity field within the bay at $t = 30.0$ is shown with arrows. The velocity vector of the vortex is illustrated by a bar starting from a dot representing the location of the vortex.

The vortex advection around the step and within the bay is determined by X_0 and Y_0. By changing X_0, the vortex-induced velocity within the bay can have different patterns. For example, the advection is northwestward when the vortex is located outside the bay to the east and is southwestward when the vortex is located to the west. By changing Y_0, the strength of the vortex advection is different. In this section, we explore the dependence on Y_0 and Δq and meanwhile keep X_0 fixed at 8π. As mentioned before, when $X_0 = 8\pi$, the zonal component of the vortex advection within the bay is completely symmetric about the bay's central axis, so any zonally asymmetric feature of the vortex–step interaction is not due to the vortex forcing but is an intrinsic nature of the system. We vary Δq between 0.5 and 2 to change the ratio of the strengths between the topography and the vortex. The initial distance between the vortex and the step is varied between 0.5 and 2, and the latter is 4 times the depth of the bay. How the dependence on Y_0 and Δq are affected by the minimum shelf width d_1 is also explored by setting d_1 equal to 0.01 or 0.2.

In situations of small minimum shelf width, when Δq is twice the vortex circulation and $Y_0 = 1.0$ (Fig. 11a), the wave propagation mechanism becomes stronger than that in the standard case: the initial crest of the PV front displays a strong tendency for eastward motion at $t = 12.0$

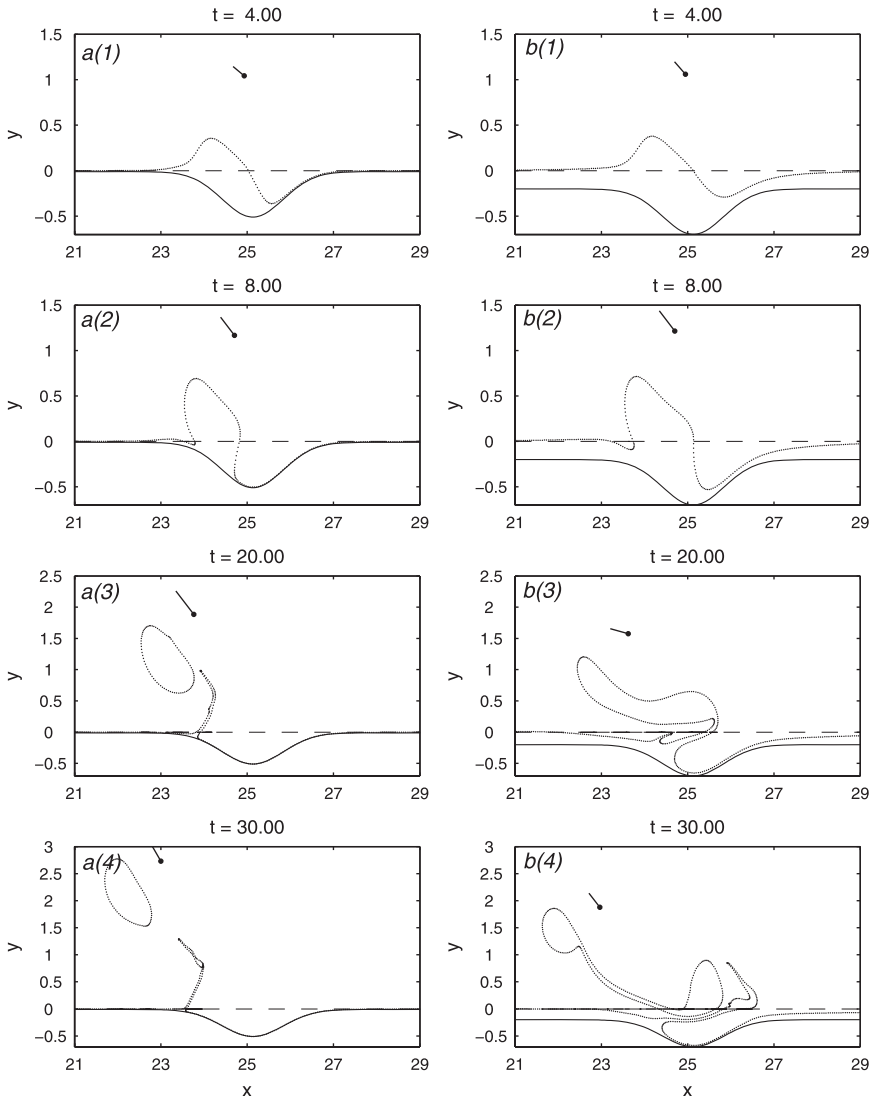

FIG. 10. Time evolution of the PV front (lines made up of dots) in anticyclone-induced cases with ($X_0 = 8\pi$, $Y_0 = 1.0$), $\Delta q = 1$, and $d_1 =$ (a) 0.01 and (b) 0.2: (top to bottom) $t = 0.00$, 8.00, 20.00, and 30.00.

compared with Fig. 9a. A topographic cyclone forms and detaches from the bay shortly after $t = 30.0$ (not shown) and its volume is about half of that in Fig. 9a, suggesting the suppression effect of increasing Δq to the cross-shelf transport.

Conversely, decreasing Δq from its standard value (Fig. 11b) strengthens the vortex advection. The initial crest extends quickly northward, approaching the forcing vortex and turning into a topographic cyclone more stretched along its north–south axis, similar to that in the case without topography (Fig. 7a).

When Δq remains the same as in the standard case while the distance between the vortex and the step is decreased to the depth of the bay (Fig. 12b), the evolution of the PV front is very similar to that in the case with weaker topography, $\Delta q = 0.5$ (Fig. 11b). All the bay water is taken off the step as an isolated eddy stretched around the forcing vortex clockwise.

The case with the vortex–step distance doubled from the standard value (Fig. 12a) is not similar to the case with $\Delta q = 2$ (Fig. 11a). Although the advection of the bay water by the vortex is rather weak relative to the wave mechanism, nearly all the bay water is still taken off the step as a cyclonic eddy. Because of the big distance between the forcing vortex and the topography, the newly formed cyclone is mostly affected by the deep-ocean water within the bay. Instead of moving northward with the vortex, it is slowly advected clockwise back onto the

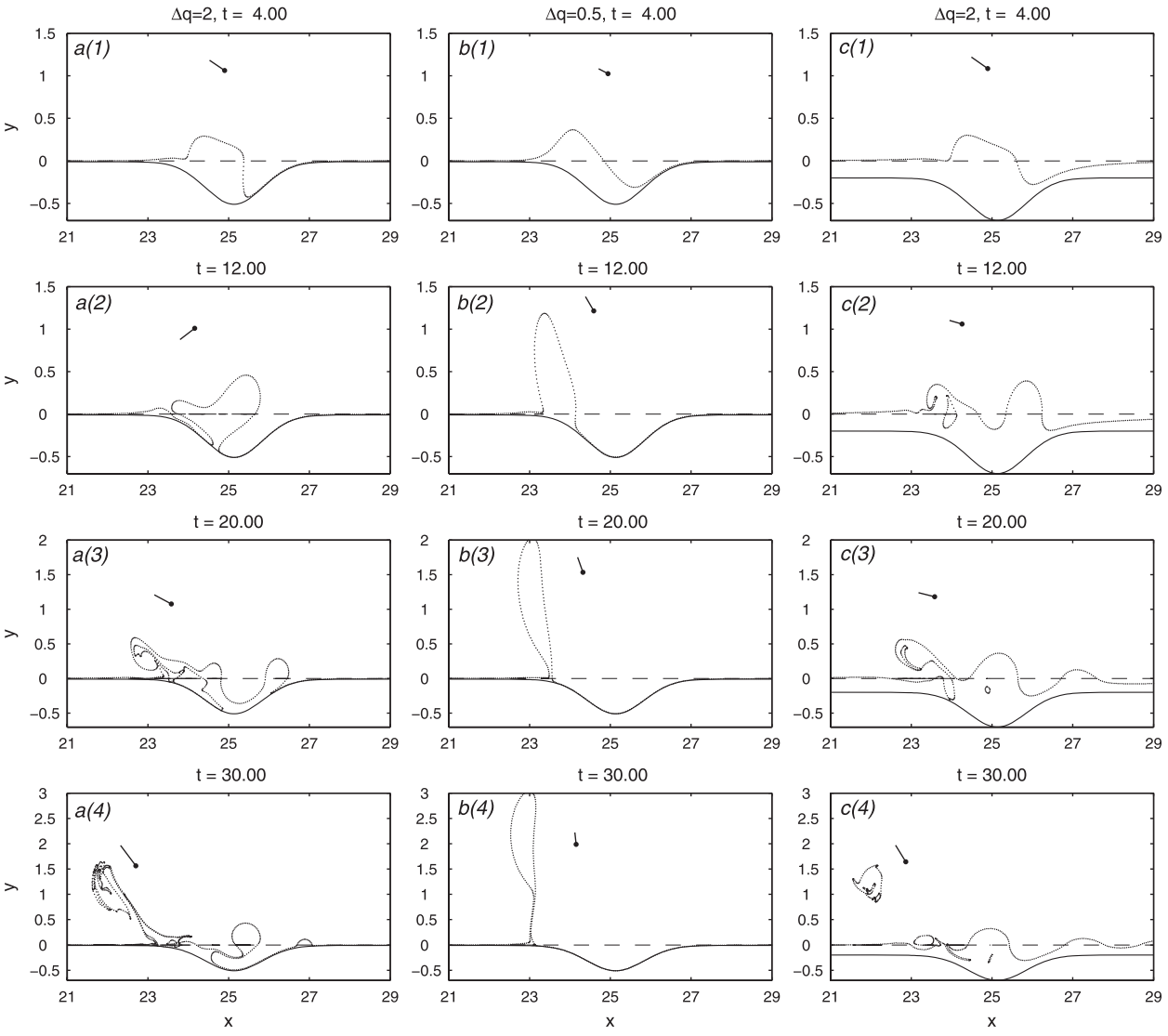

FIG. 11. Time evolution of the PV front (lines made up of dots) in anticyclone-induced cases with d_1 equal to (left),(middle) 0.01 and (right) 0.2.: (top to bottom) $t = 0.00, 12.00, 20.00$, and 30.00. The vortex's initial location is ($X_0 = 8\pi$, $Y_0 = 1.0$), same for all three cases; the PV difference across the topography Δq is 2.0 in (a),(c) but is 0.5 in (b).

shelf. The forcing vortex, on the other hand, is slowly advected anticlockwise toward the shelf.

Overall, with small d_1, decreasing the initial distance between the vortex and the step has similar effects as decreasing the height of the topography. Both variations make the vortex advection mechanism relatively strong compared with the wave propagation mechanism, and the bay water is more readily transported off the step as an isolated topographic cyclone. On the other hand, increasing Y_0 or Δq weakens the vortex's effect relative to the wave effect, the cross-shelf transport is either slow as in the case with $Y_0 = 2.0$ or not efficient as part of the bay water remains over the shelf in the case with $\Delta q = 2.0$.

In situations of $d_1 = 0.2$, the vortex–step interaction with $\Delta q = 2$ (Fig. 11c) is similar to its counterpart with small d_1 (Fig. 11a): a small topographic cyclone forms and moves away with the forcing vortex. The major differences are that, in the case with big d_1, the wave motions are more prominent and more cross-step transport is driven from outside the bay. When Y_0 instead of Δq is doubled from the standard value, the cases with small d_1 (Fig. 12a) and big d_1 (Fig. 12c) are very different. For small d_1, most of the bay water forms an isolated cyclone moving around the bay, whereas, for big d_1, wave motions are forced everywhere along the PV front but no isolated topographic cyclones are generated.

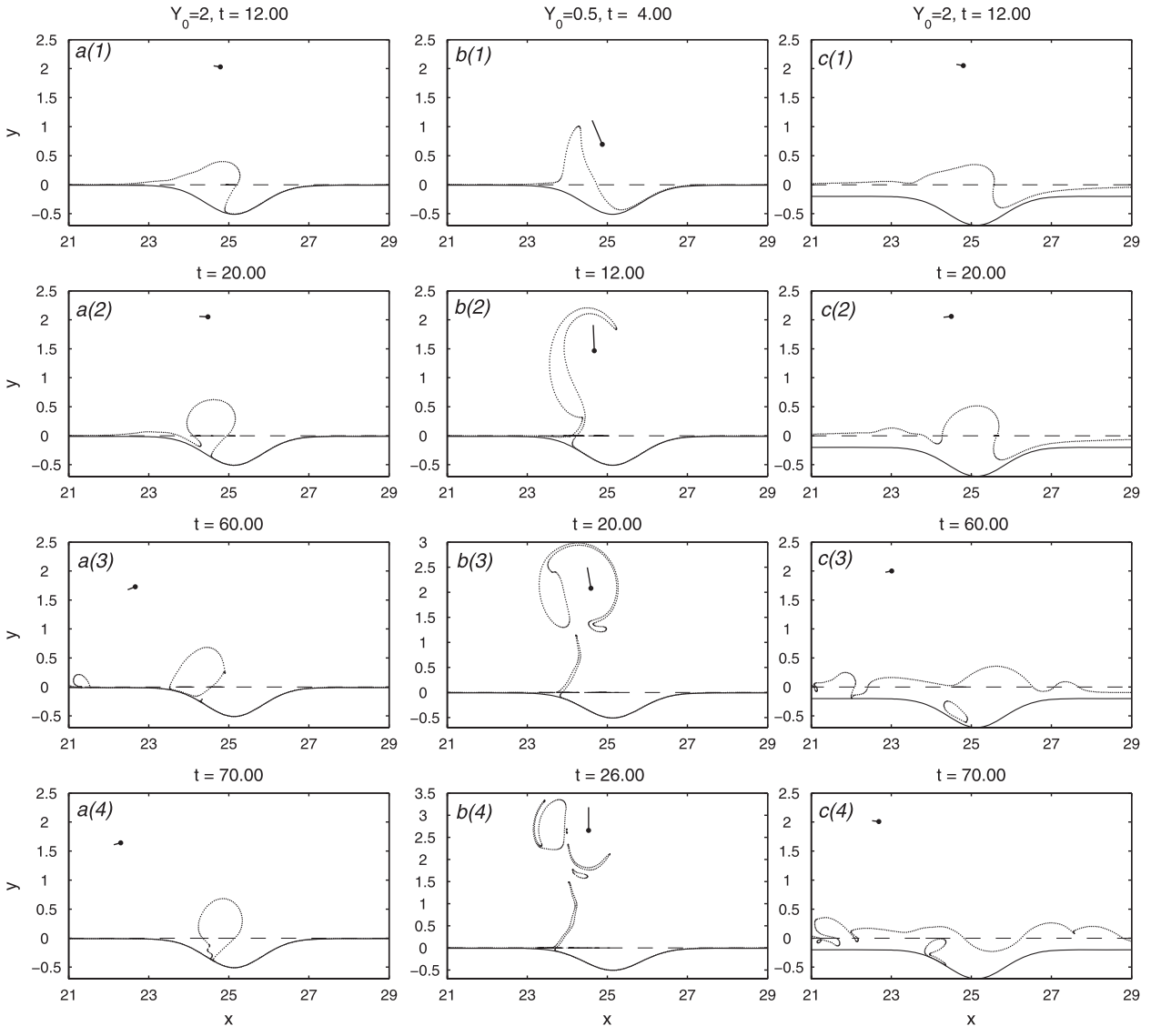

FIG. 12. Time evolution of the PV front (lines made up of dots) in anticyclone-induced cases with d_1 equal to (left),(middle) 0.01 and (right) 0.2: (top to bottom) (left) $t = 0.00, 20.00, 60.00$, and 70.00; (middle) $t = 4.00, 12.00, 20.00$, and 26.00; and (right) $t = 12.00, 20.00, 60.00$, and 70.00. The PV difference across the topography Δq is 1.0 for all three cases; the vortex's initial meridional location Y_0 is 2.0 in (a),(c) but is 0.5 in (b).

If the formation of a topographic cyclone is taken as an indication of the balance between the two competing mechanisms, there is a relatively big parameter range for both Δq and Y_0 to maintain the balance in situations of small d_1: the balance holds even when the vortex is initially located at $Y_0 = 2.0$, which is impossible for the big d_1 case. The effect of d_1 is interpreted as follows: Longer waves propagate faster, whereas short waves are left behind according to the analytical expression of the linear wave's phase speed. In the limit of zero d_1, all wave motions of the PV front are restricted to inside the bay; in other words, the longest wavelength permitted is the length of the bay opening. For large d_1, frontal waves are allowed outside the bay, and the largest wavelength can be longer than the bay opening. Therefore, the minimum shelf width puts an upper limit on the propagation speed of the frontal waves. When that limit is very low as in the case of $d_1 = 0.01$, even if the vortex is initially located far away from the step, its advection can still be faster than the wave propagations.

d. Dependence of the anticyclone-induced interactions on the initial zonal location X_0

In sections 3b and 3c, the forcing vortex initially faces the southern tip of the bay, and the zonal component of the vortex's circulation within the bay is symmetric about

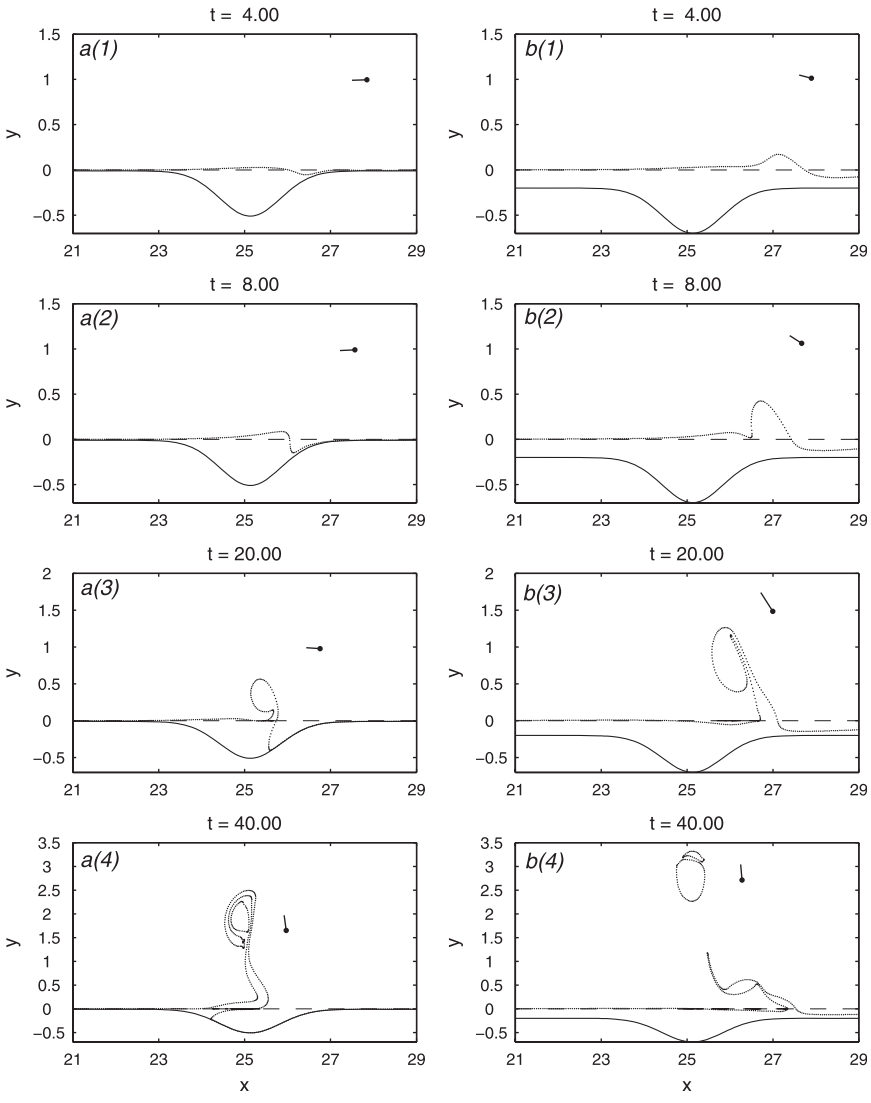

FIG. 13. Time evolution of the PV front (lines made up of dots) in anticyclone-induced cases with d_1 equal to (left) 0.01 and (right) 0.2: (top to bottom) $t = 4.00$, 8.00, 20.00, and 40.00. The vortices in both cases are initially located at ($X_0 = 8\pi + 3.0$, $Y_0 = 1.0$), and the PV difference across the topography is $\Delta q = 1.0$.

the bay's axis. In this section, we examine vortex–step interactions with vortices starting from the east of the bay by setting $X_0 = 8\pi + 3$ and keeping other parameters the same as in the standard case.

Shown in Fig. 13 are two results with different d_1. In the case with $d_1 = 0.01$, initially after $t = 0.0$, the PV front is slightly deformed seaward in the middle part of the bay opening, reflecting the clockwise advection by the vortex. Near the eastern edge of the bay, the front is indented shoreward along the boundary, reflecting the effect of the wave–boundary interactions. Both the seaward and the shoreward deformations of the PV front grow in time as the vortex translates westward toward the bay under the effect of the straight coast. At $t = 20.0$, the northeastern corner of the bay is emptied with the deep-ocean water; the seaward PV deformation evolves into a head with a narrow neck connected to the shelf. Because the vortex's distance to the middle of the bay opening is farther than that in the standard case, the vortex advection appears relatively weak and the stagnant segment of the PV front starts from the midpoint of the bay opening rather than near the western edge of the bay as in Fig. 9a. As a result, the PV front to the west of the head remains nearly parallel with the topography. To the east of the head, the shoreward PV deformation continues to extend westward, squeezing the bay water into the neck. As the head is

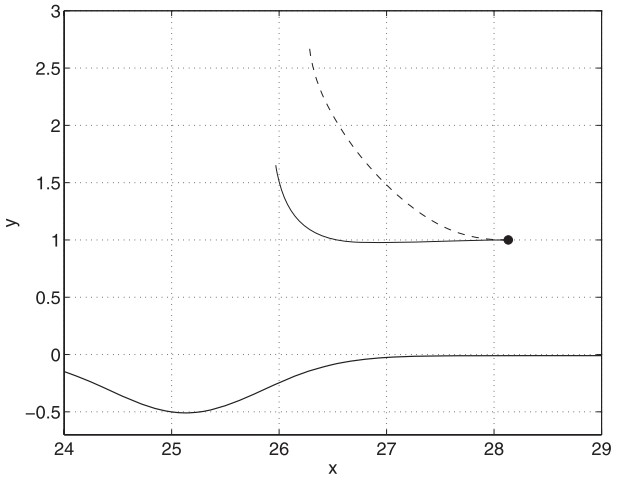

FIG. 14. Vortex trajectories in the case with d_1 equal to 0.01 (solid) and 0.2 (dashed) in Fig. 13. The thick solid line illustrates the southern boundary of the domain.

advected northward by the vortex, it also rolls anticlockwise, so the neck is stretched into a filament, circling around the head. By time $t = 40.0$, the bay is filled with the deep-ocean water, except near the northwestern edge, and the head, which is still connected to the shelf, has been advected very far into the deep ocean.

When the shelf width is 0.2 outside the bay, strong PV deformations occur right to the south of the forcing vortex rather than inside the bay. The initial seaward deformation of the PV front quickly grows into a big head, much larger than that in the previous case. The big head advects the vortex northward from the coast and soon detaches from the front. Meanwhile, the PV front inside the bay remains flat and the bay water is intact.

The case with small d_1 successfully demonstrates the vortex–step interaction with the vortex being advected westward along the wall as shown by its trajectory in Fig. 14. During the process, the vortex is always to the east of the seaward deformation of the PV front, so it continuously forces the formation of the topographic cyclone. If somehow the propagation speed of the vortex along the coast is increased relative to the formation rate of the topographic cyclone, the vortex may move to the west of the seaward deformation or even move out of the zonal range of the bay before the cyclone forms, and then it no longer can support the growth of the PV deformation. In real oceans, mesoscale eddies propagate westward because of the variation of the Coriolis parameter, which is absent in the current configuration. We can simulate this effect by imposing a constant westward velocity $u_f < 0$ to the point vortex. Figure 15 shows three cases with increasing $|u_f|$ but same values of $\Delta q = 1$, ($X_0 = 8\pi + 3$, $Y_0 = 1.0$), and $d_1 = 0.01$. The out-of-bay transport is faster and more complete in the case with $u_f = -0.5$ than in the case with $u_f = 0$. When $|u_f|$ is even bigger (Figs. 15b,c), the major part of the seaward deformation of the PV front has no time to be advected far northward before the vortex quickly exits the zonal range of the bay; only its northern end is stretched into a long and thin filament encircling the fast-moving vortex. At $t = 40.0$, most of the bay water lingers around the bay opening and probably returns to the shelf at a later time under the forcing of the deep-ocean water within the bay.

4. Conclusions

This paper examined the interaction between a barotropic point vortex and a zonally orientated steplike topography. Compared with prior literature on eddy–topography interactions, the novel feature of this study is the consideration of the shelf geometry, which is a bay enclosed by the curved coast and the step. Because of the curvature of the coast, the shelf is narrow near the two zonal ends of the bay and wide in between. Waves propagating along the step tend to be blocked by the coast over the narrower shelf. This results in nonlinear wave–boundary interaction, inducing strong out-of-bay transport in the form of detached crests of the PV front. Because waves propagate in only one direction, the strong out-of-bay transport only occurs near one side boundary of the bay. In a coastal region like the western Antarctic Peninsula shelf and Marguerite Bay, waves supported by the topography propagate westward, and their interaction with the western boundary of the bay may potentially contribute to the CDW intrusion onto the shelf and into the bay. The eastern area of Marguerite Bay is much less vulnerable to the wave–boundary interaction and may be a retention region of Antarctic krill. Similar phenomenon may also be found in other coastal areas where the shelf width decreases in the propagation direction of the topographic Rossby waves such as the Gulf of Mexico and the Gulf of Alaska.

Our understanding of the fundamental mechanism benefits a lot from the simplifications made in the model, such as the barotropic assumption and the use of the step topography, but the model is also limited by these simplifications. Any quantitative comparison between the model and the real ocean has to be made very carefully because of the following reasons: First, the decay length scale of the vortex under the barotropic assumption is quite large compared with that in the baroclinic ocean, making the vortex's effect readily reach far into the bay and easily replace all the bay water with the deep-ocean water. This is a striking feature of the model results but may not be true for the real ocean. Zhang (2009) considers the interaction between a baroclinic eddy and a

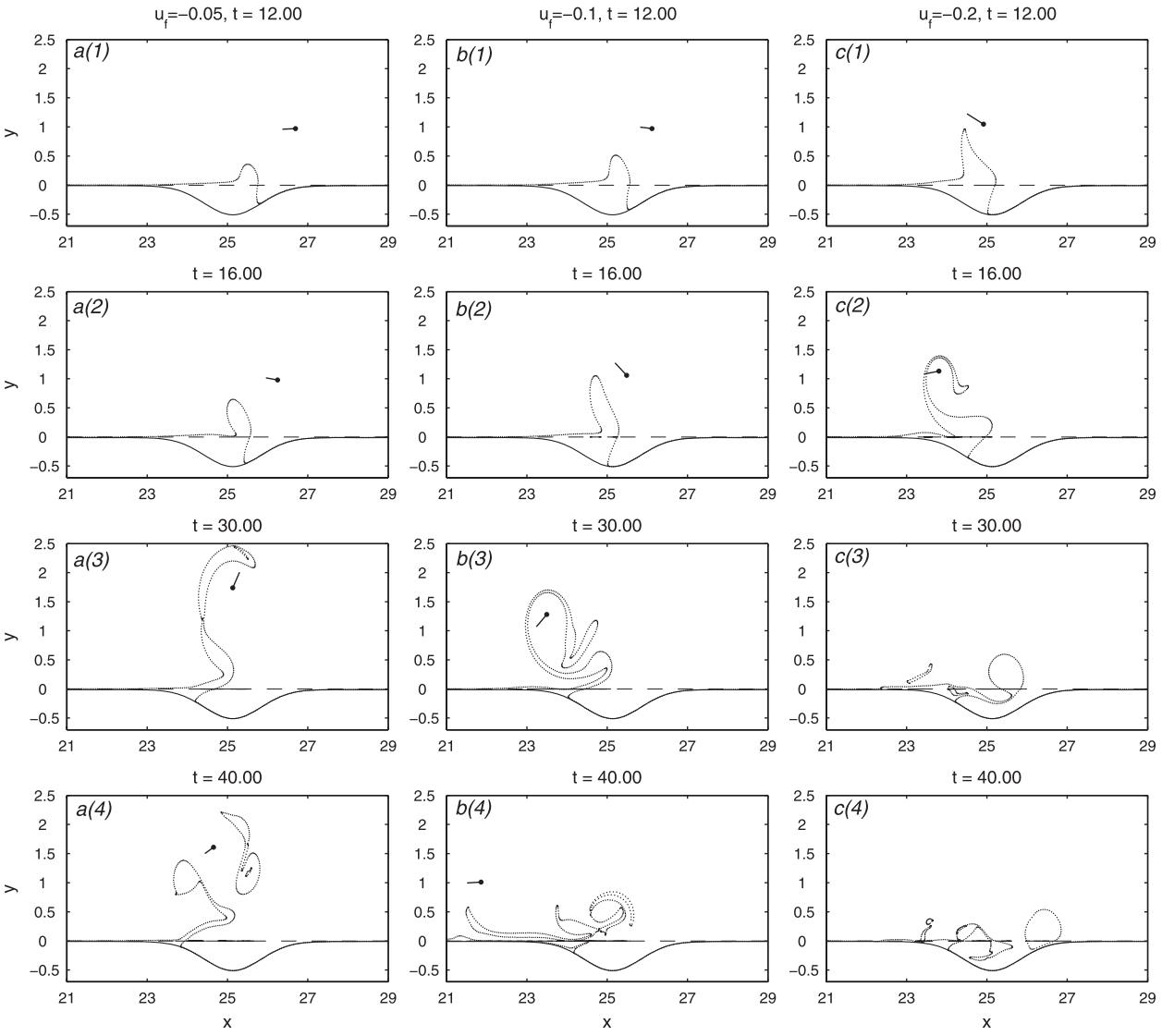

FIG. 15. Time evolution of the PV front (lines made up of dots) in anticyclone-induced cases with $d_1 = 0.01$, ($X_0 = 8\pi + 3.0$, $Y_0 = 1.0$), and $\Delta q = 1.0$. The anticyclonic vortex translates westward with a prescribed velocity u_f, which is (left) -0.05, (middle) -0.1, and (right) -0.2: (top to bottom) $t = 12.00$, 16.00, 30.00, and 40.00.

smooth slope with a bay-shaped shelf, in which the features seen in the present paper can still be identified, but the bay becomes less susceptible to replacement because of the shorter range of baroclinic fields and because a smoother topographic slope (as opposed to a step) generates waves interacting more with other parts of the slope than with the shelf. Second, as shown by results in the paper, the minimum distance between the shelf break and the coast affects the intensity of the nonlinear wave–boundary interaction and hence the resultant out-of-bay transport. When the distance is large or the shelf width changes more gradually, waves forced by a single eddy will more readily propagate through the narrow-shelf region and strong cross-isobath transport is less likely to happen. In the baroclinic interaction between a single eddy and the topography (Zhang 2009), the wave–boundary interaction is hardly noticeable because of the short decay range of the baroclinic eddy. However, when the intermittent forcing of the ACC is included in the model, topographic waves can be excited intermittently and probably at multiple sites along the bay opening. Then, the cumulative effect of the wave–boundary interaction can still bring large amount of water out of the bay (Zhang 2009; ZPF). In this sense, although the barotropic model is highly abstracted from the oceanographic condition, it is crucial in demonstrating the mechanism that is essential for the

out-of-bay transport under the continuous forcing of the open-ocean current.

Another major result of our study is that the single propagation direction of topographic Rossby waves causes fundamental difference between the anticyclone- and cyclone-induced interactions. In anticyclone-induced interactions, waves propagate against the advection by the vortex. As a consequence of the balance between the two opposing tendencies, a topographic cyclone forms from the step, taking a large amount of the shelf water into the deep ocean. In cyclone-induced interactions, however, the PV front is quickly advected because of both the vortex advection and the wave propagation; a topographic cyclone forms only because of the breaking of waves and the cross-shelf transport is weaker than in the anticyclone case. The fundamental difference between the two cases is independent on the stratification of the model ocean but is most clearly demonstrated in the barotropic model with a single PV front generated by a steplike topography.

Acknowledgments. The authors thank S. Meacham for the original contour surgery code. Y. Zhang acknowledges the support of the MIT-WHOI Joint Program in Physical Oceanography, NSF OCE-9901654 and OCE-0451086. J. Pedlosky acknowledges the support of NSF OCE-9901654 and OCE-0451086.

APPENDIX A

Free, Linear Topographic Rossby Waves

If motions are excited near the step and friction effects on PV are negligible, water columns crossing the step conserve PV by generating relative vorticity and the PV front is deformed from $y = 0$ with new position $y = l$. Water columns between the step and the seaward-deformed front ($0 < y < l$) have their thickness stretched from h_2 (shallow-area value) to h_1 (deep-area value); water columns between the step and the shoreward-deformed front ($l < y < 0$) have their thickness squeezed from h_1 to h_2. Functions H_{new} and H_{old} are defined to represent the original and the new thickness of water columns that have crossed the step from either side,

$$\begin{aligned} H_{\text{old}} &= h_2 + (h_1 - h_2)\Theta(y - l), \\ H_{\text{new}} &= h_2 + (h_1 - h_2)\Theta(y), \end{aligned} \tag{A1}$$

where Θ is the Heaviside function. The conservation of PV requires

$$\frac{f_0}{H_{\text{old}}} = \frac{f_0 + \nabla^2\psi}{H_{\text{new}}}, \tag{A2}$$

from which the relative vorticity is solved as

$$\begin{aligned} \nabla^2\psi &= \frac{f_0(H_{\text{new}} - H_{\text{old}})}{H_{\text{old}}}, \\ &= \frac{f_0}{H_{\text{old}}}(h_1 - h_2)[\Theta(y) - \Theta(y - l)]. \end{aligned} \tag{A3}$$

Under the assumption that l is small, we can expand $\Theta(y - l)$ into Taylor series around 0 and only keep the first two terms: $\Theta(y - l) \approx \Theta(y) - l\delta(y)$. For small step topography across which the depth difference is small compared with the water depth on both sides, f_0/H_{old} can be approximated as f_0/H_0, which is independent of space. Now, once we know the meridional location of the front, the relative vorticity can be solved from a simple relation,

$$\nabla^2\psi = \Delta q l \delta(y), \tag{A4}$$

where $\Delta q = (f_0/H_0)(h_1 - h_2)$ is the PV jump across the topography. The velocity field is related to the streamfunction as follows:

$$\begin{aligned} u &= -\frac{\partial\psi}{\partial y}, \\ v &= \frac{\partial\psi}{\partial x}, \end{aligned} \tag{A5}$$

and the PV front is advected by the velocity field,

$$\frac{\partial l}{\partial t} + u_l\frac{\partial l}{\partial x} = v_l, \tag{A6}$$

where u_l and v_l are velocities on the front. With small l relative to the zonal length of the PV front deformation, the above equation is linearized as

$$\frac{\partial l}{\partial t} = v_0, \tag{A7}$$

where v_0 is velocity at $y = 0$. Integrating (A4) in y from $-\epsilon$ to ϵ yields

$$\int_{-\epsilon}^{\epsilon}\frac{\partial^2\psi}{\partial x^2}\,dy + \left(\frac{\partial\psi}{\partial y}\right)_{-\epsilon}^{\epsilon} = \int_{-\epsilon}^{\epsilon}\Delta q l\delta(y)\,dy. \tag{A8}$$

In the limit of $\epsilon \to 0$, the first term in (A8) vanishes, and the zonal velocity has a jump across the step,

$$\left(\frac{\partial\psi}{\partial y}\right)_{-\epsilon}^{\epsilon} = \Delta q l, \tag{A9}$$

although ψ itself is continuous at $y = 0$. Because the region is only bounded by the southern boundary, the physical

solution of ψ is 0 at $y = 0$ and is finite as y goes to infinity. If B_s varies more slowly in x than the phase of the wave does, we can apply the WKB approximation method and seek a solution in the form of $l = l_0(x)\exp[i\theta(x) - i\omega t] + \text{c.c.}$, where c.c. denotes the complex conjugate. Both the amplitude l_0 and the wavenumber $k = d\theta/dx$ are slow functions of x. The solution of ψ is expected to be $\psi = A\exp[i\theta(x) - i\omega t]\phi(y) + \text{c.c.}$. Substituting this solution in (A4) in the flat-bottomed region, we have

$$\left[\frac{\partial^2 A}{\partial x^2} + i\left(2k\frac{\partial A}{\partial x} + A\frac{\partial k}{\partial x}\right) - k^2 A\right]\phi + A\frac{\partial^2 \phi}{\partial y^2} = 0. \quad \text{(A10)}$$

Because k and A are weak functions of x, $dk/dx \ll k$ and $dA/dx \ll A$ The imaginary terms of (A10) are much smaller than real terms, and to leading order we obtain an equation describing the meridional structure of ϕ,

$$\frac{\partial^2 \phi}{\partial y^2} - k^2\phi = 0. \quad \text{(A11)}$$

According to the boundary condition, $\phi(y > 0) = A_n e^{-ky}$ and $\phi(y < 0) = A_s \sinh k(y - B_s)$. The continuity of ψ and the discontinuity of the zonal velocity at $y = 0$ require that

$$\begin{aligned} \psi_n &= \psi_s \quad \text{at} \quad y = 0, \\ \left[\frac{\partial \psi_n}{\partial y}\right]_{y=0} - \left[\frac{\partial \psi_s}{\partial y}\right]_{y=0} &= \Delta q l_0 \quad \text{at} \quad y = 0, \end{aligned} \quad \text{(A12)}$$

from which we obtain $A_n = (\Delta q l_0/2k)(e^{2kB_s} - 1)$ and $A_s = -(\Delta q l_0/k)e^{kB_s}$. Substituting solutions of l and υ_0 in (A7), we get the dispersion relation $\omega = (\Delta q/2)(1 - e^{2kB_s})$.

The imaginary part of (A10) describes the slow variation of the amplitude A with the wavenumber k,

$$\frac{\partial (Ak^{1/2})}{\partial x} = 0. \quad \text{(A13)}$$

APPENDIX B

Choice of the Channel Length

The zonally reentrant channel is meant to be a simplification of the circular path of the Antarctic Circumpolar Current. In numerical calculations, the channel length is finite and its value is important to ensure that the velocity field induced by a point vortex in the channel is close to that in an annulus.

According to our solution method (appendix C), the circulation of a single vortex located at (X_0, Y_0) in a periodic channel extending from $x = 0$ to $x = a$ is equivalent to the circulation generated by an infinite array of equal-strength vortices lying along Y_0 in an infinite channel and spaced a distance a apart. Near the string of vortices, the velocity is mostly determined by the closest vortex and is less affected by other vortices. Farther away from the string, vortices would appear more closely spaced. When the distance to the string is large enough, the distance between any two vortices is negligible and the circulation of the vortex string becomes close to that of a vortex sheet: the velocity normal to the sheet (the meridional velocity) is zero, but the tangential velocity (the zonal velocity) is constant and reverses sign across the vortex sheet. Therefore, when the vortex is very far from the southern boundary of the channel, the velocity field near the southern boundary tends to become uniform in space. Whether this is true for the annulus and, if not, how to avoid this unrealistic behavior are the two questions we try to answer in this appendix. In doing so, we solve the velocity field generated by a single vortex in an annulus and compare it against the solution in a finite-length channel without a bay in any boundaries.

Figure B1 shows an annulus lying between two concentric circles with radii r_1 and r_2 ($r_1 < r_2$). A vortex with strength Γ is located at (X_0, Y_0) in the annulus. Instead of solving the problem directly in circular coordinate, we use a transformation $z = e^{\zeta}$, where $z = x + iy$ is a complex variable in the space of the annulus and $\zeta = \kappa + i\eta$ is a variable in a new space (Fig. B2). Under this transform, any infinitely long straight line extending parallel with η axis in ζ space turns into a circle in the original z space. We first solve the Green's function within a channel between two straight lines in ζ space and transform the solution back to the z space. Suppose the two straight lines cross κ axis at $(a_1, 0)$ and $(a_2, 0)$ ($a_2 > a_1$) and the vortex is located in the channel at (κ_0, η_0), then the complex velocity generated in the ζ plane is $\tilde{W} = \tilde{u} - i\tilde{v} = -(i\Gamma/4\pi h)[\cot(\pi/2h)(\zeta - \zeta_0^+) - \cot(\pi/2h)(\zeta - \zeta_0^-)]$, where $h = a_2 - a_1$ is the width of the channel, $\zeta_0^+ = \kappa_0 + i\eta_0$ is the position of the vortex, and $\zeta_0^- = (2a_1 - \kappa_0) + i\eta_0$ is the symmetric point of ζ_0^+ about the western boundary of the meridional channel. The complex velocity W within the channel in the z plane is, according to the rules of conformal mapping, $W = \tilde{W}/(dz/d\zeta)$, and $a_1 = \ln(r_1)$, $a_2 = \ln(r_2)$, and $\zeta_0 = \ln(z_0)$. Shown in Fig. B3 are magnitudes of vortex-induced velocity along the inner circle of an annulus with two radii $r_1 = 10$ and $r_2 = 100$. The x axis in each panel shows the angle of the vector originating from ($x = 0$, $y = 0$) and ending at a point on the inner circle. Angle $\theta = -\pi$ corresponds to a point located on the negative x axis. As θ increases, the corresponding point moves clockwise along the inner circle. In both panels, the vortex is located on the positive x axis and has the same strength $\Gamma = -1$; its

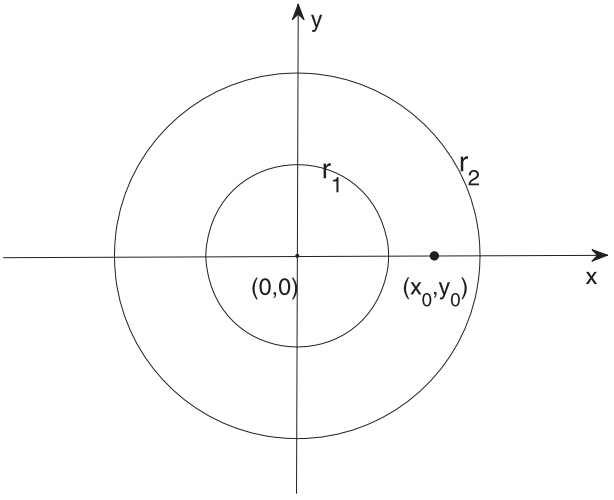

FIG. B1. A schematic of an annulus in z space.

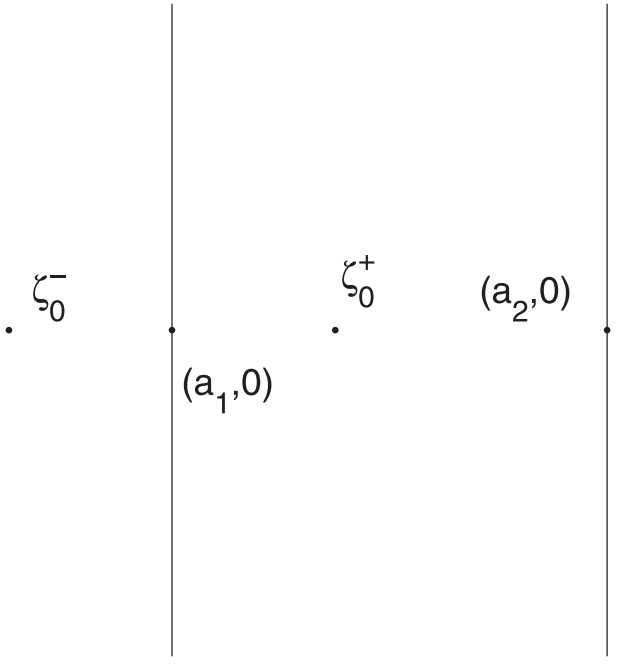

FIG. B2. A channel in ζ space with two walls crossing respectively the point at $(a_1, 0)$ and $(a_2, 0)$.

distance to the inner circle is 1 in Fig. B3a and 20 in Fig. B3b. The velocity magnitude is at a maximum right to the east of the vortex and declines away from the positive real axis. In the first panel, the flow magnitude drops quickly and becomes zero after one-quarter of the circle. In the second panel, the flow magnitude declines much slower and is nonzero everywhere, including at the farthest point $(-30, 0)$. Nevertheless, the distribution of the magnitude along the circle is far from uniform, which is only obtainable when the ratio of the two lengths, the distance between the vortex and the inner circle and the radius of the inner circle, goes to infinity. For a periodic channel with finite length $a = 2\pi$, the flow near the southern boundary becomes constant once the distance between the vortex and the boundary is about 4. To avoid the uniform velocity near the southern boundary in the zonal channel, we have to make sure the channel length a is much larger than the maximum vortex–topography distance that is of interest. The choice of $a = 16\pi$ is the largest affordable value allowed by our computational resource.

APPENDIX C

Solution Methodology

The problem is solved using the contour dynamics approach (Stern and Flierl 1987; Wang 1992). The basic strategy (Zhang 2009) is to first find the streamfunction

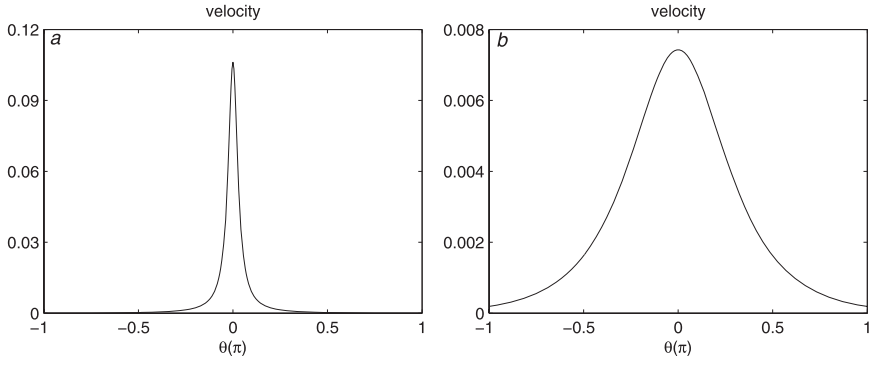

FIG. B3. The magnitude of the velocity along the inner circle of the annulus when the vortex is located (a) at $(11, 0)$ and (b) at $(30, 0)$ in z space. Here, θ denotes the angle between the vector originating from the origin and ending at the inner circle of the annulus and the x axis, on which the vortex is located.

satisfying the following nondimensional equation and boundary conditions,

$$\nabla^2\psi = q + \delta(x - X, y - Y),$$
$$\psi = 0 \quad \text{on } B_n \text{ and } B_s,$$
$$\psi(x + a, y) = \psi(x, y). \tag{C1}$$

Once the streamfunction is found, the velocity field is determined from the relation $u = -\partial\psi/\partial y, v = \partial\psi/\partial x$ and is integrated for the position of the PV front as well as the point vortex at the next time step,

$$\frac{\partial l}{\partial t} - \frac{\partial\psi(x,l)}{\partial y}\frac{\partial l}{\partial x} = \frac{\partial\psi(x,l)}{\partial x} \quad \text{and} \tag{C2}$$

$$\frac{dX}{dt} = -\frac{\partial\psi(X,Y)}{\partial y}$$
$$\frac{dY}{dt} = \frac{\partial\psi(X,Y)}{\partial x}. \tag{C3}$$

We decompose ψ into a particular solution ψ_p and a homogeneous solution ψ_h. Both are periodic in x but satisfy different equations and boundary conditions,

$$\nabla^2\psi_p = q + \delta(x - X, y - Y), \tag{C4}$$

$$\nabla^2\psi_h = 0, \quad \text{and} \tag{C5}$$

$$\psi_h = -\psi_p \quad \text{on } B_n \text{ and } B_s. \tag{C6}$$

For a distributed source as $q(x, y)$, the Poisson's Eq. (C4) is solved via the Green's function method: that is, finding the Green's function $G(x, y, \xi, \eta)$ for the equation $\nabla^2 G = \delta(x - \xi, y - \eta)$ and integrating G over the whole source area A to get $\psi_p = \iint_A q(\xi,\eta)G(x,y,\xi,\eta)\,d\xi\,d\eta$. Because of the quasigeostrophic approximation, the source function q is $\Delta q = (f/H_0)(h_1 - h_2)$ to the north of the step and $-\Delta q$ to south of the step. The previous integral is therefore reduced to $\psi_p = \Delta q \iint_{A^+} G(x, y, \xi, \eta)\,d\xi\,d\eta - \Delta q \iint_{A^-} G(x, y, \xi, \eta)\,d\xi\,d\eta$, where A^+ denotes the area between the step and the seaward-deformed (northward, $l > 0$) front and A^- denotes the area between the step and the shoreward-deformed (southward, $l < 0$) front. To find the zonally periodic Green's function corresponding to a monopole at (ξ, η), we consider a domain extending from $-\infty$ to ∞ in x. Within the domain, an infinite number of monopoles including the original one, each of which has the same strength and the same meridional location, are lined up and spaced a apart. In the complex plane $z = x + iy$, the complex potential of a single monopole at $z_0 = \xi + i\eta$ is $W = -i/2\pi \ln(z - z_0)$ and the velocity is $dW/dz = u - iv = -i/2\pi(z - z_0)$. Therefore, the velocity field induced by the string of monopoles located as $z_0 + na, n = 0, \pm1, \pm2\ldots$ is

$$u - iv = \sum_{n=-\infty}^{n=\infty} -\frac{i}{2\pi[z - (z_0 + na)]}. \tag{C7}$$

Equivalently, (C7) can be written as a cotangent function, which, when $a = 2m\pi$ (m is any positive integer), is

$$u - iv = -\frac{i}{4m\pi}\cot\left(\frac{z - z_0}{2m}\right). \tag{C8}$$

The streamfunction is therefore

$$G(x, y, \xi, \eta) = \mathrm{Im}\left[\frac{i}{2\pi}\ln\left(\sin\frac{z - z_0}{2m}\right)\right]. \tag{C9}$$

Because derivatives of Green's function with respect to x and y can be related to those to ξ and η, $\partial G/\partial y = -\partial G/\partial\eta$, $\partial G/\partial x = -\partial G/\partial\xi$, the area integrals of G can be simplified to integrals along boundaries of all source areas,

$$\begin{aligned} u_{\mathrm{pF}} &= \Delta q \iint_{A^+} \frac{\partial}{\partial\eta} G\,d\xi\,d\eta - \Delta q \iint_{A^-} \frac{\partial}{\partial\eta} G\,d\xi\,d\eta \\ &= \Delta q \left(\oint_{y=0} G\,d\xi - \oint_1 G\,d\eta\right) \\ v_{\mathrm{pF}} &= -\Delta q \iint_{A^+} \frac{\partial}{\partial\xi} G\,d\xi\,d\eta + \Delta q \iint_{A^-} \frac{\partial}{\partial\xi} G\,d\xi\,d\eta \\ &= -\Delta q \oint_1 G\,d\eta, \end{aligned} \tag{C10}$$

where F means the velocity is forced by the front deformation. The velocity induced by the point vortex is simply

$$u_{\mathrm{pV}} - iv_{\mathrm{pV}} = -\frac{i}{4m\pi}\cot\left(\frac{z - z_0}{2m}\right), \tag{C11}$$

where $z_0 = X + iY$.

In seeking the homogeneous solution, we put N monopoles outside the model domain. Among them, N_1 are lined up next to the northern boundary B_n and $N - N_1$ are next to the southern boundary B_s. Because, they are located outside the domain, the streamfunction related to these monopoles satisfies the homogeneous equation within the domain. The strengths of these N monopoles are determined by requiring the total circulation, the circulation induced by sources inside the domain and those outside the domain, has zero normal component at N locations on the two boundaries (N_1 on $y = B_n$ and $N - N_1$ on $y = B_s$). As long as the PV front position and the point

vortex position are known, we know the normal velocity of the particular solution at these N locations. The result is written as an N by 1 column vector denoted as $\mathbf{V}_0$. If every monopole outside the domain has unit strength, we can write an N by N matrix $\mathbf{M}$. Each row of $\mathbf{M}$ is the array of the normal velocity at one single location induced by the N monopoles; each column of $\mathbf{M}$ is the array of the normal velocity at N different locations induced by one single monopole. To cancel the normal velocity of the particular solution on boundaries, strengths of monopoles outside the domain cannot be uniformly one. We define an N by 1 unknown column vector $\mathbf{P}$ to represent the strengths of those monopoles; it satisfies the relation

$$\mathbf{MP} = -\mathbf{V}_0, \tag{C12}$$

and the vector P is found via inverting the matrix $\mathbf{M}$,

$$\mathbf{P} = -\mathbf{M}^{-1}\mathbf{V}_0. \tag{C13}$$

The velocity field $\mathbf{u}_h$ forced by these monopoles can now be calculated. Both $\mathbf{u}_p$ and $\mathbf{u}_h$ are continuous across the topography, so the complete solution for (C1) is obtained by simply adding them together. The new positions of the front and the point vortex are integrated in time in (C2) and (C3).

REFERENCES

Bell, G. I., 1990: Interaction between vortices and waves in a model of geophysical flow. *Phys. Fluids,* **2,** 575–586.

——, and L. G. Pratt, 1992: The interaction of an eddy with an unstable jet. *J. Phys. Oceanogr.,* **22,** 1229–1244.

Chapman, D. C., and K. H. Brink, 1987: Shelf and slope circulation induced by fluctuating offshore forcing. *J. Geophys. Res.,* **92,** 11 741–11 759.

Dinniman, M. S., J. M. Klinck, and W. O. Smith Jr., 2011: A model study of Circumpolar Deep Water on the West Antarctic Peninsula and Ross Sea continental shelves. *Deep-Sea Res. II,* in press, doi:10.1016/j.dsr2.2010.11.013.

Dritschel, D. G., 1988: Contour surgery: A topological reconnection scheme for extended integrations using contour dynamics. *J. Comput. Phys.,* **77,** 240–266.

Frolov, S. A., G. G. Sutyrin, G. D. Rowe, and L. M. Rothstein, 2004: Loop Current eddy interaction with the western boundary in the Gulf of Mexico. *J. Phys. Oceanogr.,* **34,** 2223–2237.

Garfield, N., and D. L. Evans, 1987: Shelf water entrainment by Gulf Stream warm-core rings. *J. Geophys. Res.,* **92,** 13 003–13 012.

Hofmann, E. E., J. M. Klick, D. P. Costa, K. L. Daly, J. J. Torres, and W. R. Fraser, 2002: U.S. Southern Ocean Global Ocean Ecosystems Dynamics program. *Oceanography,* **15,** 64–74.

Klinck, J. M., 1998: Heat and salt changes on the continental shelf west of the Antarctic Peninsula between January 1993 and January 1994. *J. Geophys. Res.,* **103,** 7617–7636.

——, E. E. Hofmann, R. C. Beardsley, B. Salihoglu, and S. Howard, 2004: Water-mass properties and circulation on the west Antarctic Peninsula continental shelf in austral fall and winter 2001. *Deep-Sea Res. II,* **51,** 1925–1946.

Louis, J. P., and P. C. Smith, 1982: The development of the barotropic radiation field of an eddy on a slope. *J. Phys. Oceanogr.,* **12,** 56–73.

Moffat, C., B. Owens, and R. C. Beardsley, 2009: On the characteristics of Circumpolar Deep Water intrusions to the west Antarctic Peninsula Continental Shelf. *J. Geophys. Res.,* **114,** C05017, doi:10.1029/2008JC004955.

Orsi, A. H., T. Whitworth, and W. D. Nowlin, 1995: On the meridional extent and fronts of the Antarctic Circumpolar Current. *Deep-Sea Res.,* **42,** 641–673.

Prezelin, J. R., E. E. Hofmann, C. Mengelt, and J. M. Klinck, 2000: The linkage between Upper Circumpolar Deep Water (UCDW) and phytoplankton assemblages on the west Antarctic Peninsula continental shelf. *J. Mar. Res.,* **58,** 165–202.

Smith, D. A., E. E. Hofmann, J. M. Klinck, and C. M. Lascara, 1999: Hydrography and circulation of the west Antarctic Peninsula continental shelf. *Deep-Sea Res.,* **46,** 951–984.

Smith, D. C., and J. J. O'Brien, 1983: The interaction of a two-layer isolated mesoscale eddy with bottom topography. *J. Phys. Oceanogr.,* **13,** 1681–1697.

Stern, M. E., 1991: Entrainment of an eddy at the edge of a jet. *J. Fluid Mech.,* **228,** 343–360.

——, and G. R. Flierl, 1987: On the interaction of a vortex with a shear flow. *J. Geophys. Res.,* **92,** 10 733–10 744.

Wang, X., 1992: Interaction of an eddy with a continental slope. Ph.D. thesis, Massachusetts Institute of Technology/Woods Hole Oceanographic Institution, 216 pp.

White, A. J., and N. R. McDonald, 2004: The motion of a point vortex near large-amplitude topography in a two-layer fluid. *J. Phys. Oceanogr.,* **34,** 2808–2824.

Zhang, Y., 2009: Slope/shelf circulation and cross-slope/shelf transport out of a bay driven by eddies from the open ocean. Ph.D. thesis, Massachusetts Institute of Technology/Woods Hole Oceanographic Institution, 222 pp.